LUND UNIVERSITY

Active Stabilization of Thermoacoustic Oscillation

Kjaer, Martin Ansbjerg

2005

Document Version:
Publisher's PDF, also known as Version of record

Link to publication

Citation for published version (APA):
Kjaer, M. A. (2005). *Active Stabilization of Thermoacoustic Oscillation.* [Licentiate Thesis, Department of Automatic Control]. Department of Automatic Control, Lund Institute of Technology, Lund University.

Total number of authors:
1

General rights
Unless other specific re-use rights are stated the following general rights apply:
Copyright and moral rights for the publications made accessible in the public portal are retained by the authors and/or other copyright owners and it is a condition of accessing publications that users recognise and abide by the legal requirements associated with these rights.
• Users may download and print one copy of any publication from the public portal for the purpose of private study or research.
• You may not further distribute the material or use it for any profit-making activity or commercial gain
• You may freely distribute the URL identifying the publication in the public portal

Read more about Creative commons licenses: https://creativecommons.org/licenses/

Take down policy
If you believe that this document breaches copyright please contact us providing details, and we will remove access to the work immediately and investigate your claim.

LUND UNIVERSITY

PO Box 117
221 00 Lund
+46 46-222 00 00

Active Stabilization of Thermoacoustic Oscillation

Martin Ansbjerg Kjær

Department of Automatic Control
Lund University
Lund, December 2005

Til Marianne

Department of Automatic Control
Lund University
Box 118
SE-221 00 LUND
Sweden

ISSN 0280–5316
ISRN LUTFD2/TFRT--3239--SE

© 2005 by Martin Ansbjerg Kjær. All rights reserved.
Printed in Sweden,
Lund University, Lund 2005

Acknowledgments

First of all, I would like to thank my supervisor, Rolf Johansson, who's impressive knowledge in wide ranging areas has been an inspiration through out my time at the Department of Automatic Control. Also, I am grateful for the enthusiasm he has put into the supervision. Also, I owe my gratitude to my co–supervisor, Anders Robertsson, who, despite of a full calender, always seems to find time.

Through all the time I have spend at the laboratory at the Department of Heat and Power Engineering, Lund University, I have come to know a lot of fine people. For the help to construct the test rig I gladly acknowledge Fredrik Hermann and Ingjald Andreasson, without who I would still struggle to get the fire going. Thank you both so much. Jens Klingmann, Rolf Gabrielsson and Raik Orbay are also thanked for the discussions on the field of gas–turbines and combustion chambers. From the Department of Fluid Dynamics I owe my gratitude to Christophe Duwig for his help and discussions on the nature of flames. I hope for a continuing cooperation between our departments.

Gratitude goes to all my colleagues at my own department—the Department of Automatic Control. It is a pleasure to work at an institution so well organized and with so friendly and skilled people. A special thanks to Karl Johan Åström for his inputs and discussions. I am grateful to Leif Andersson, Anders Blomdell, and Rolf Braun for their help with computers, laboratory equipment, and inspiration to practical solutions. I would wish all departments could have such fine technical staff as we do. Brad Schofield and Oskar Nilsson are acknowledged for their help on my manuscript. The girls on the fifth floor (tjejerna på 5:e våning), Britt-Marie Mårtensson, Eva Schildt, and Agneta Tuszynski, holds a special place in my heart. No one does as much to form a good social and well organized work–environment at the department as them.

CECOST is acknowledged for the financial support and for the interesting annual meetings serving interesting insight into various fields, such as laser diagnostics, fluid mechanics, and bio fuel. Christian Troger and Vladimir Milosavljevich of Siemens Industrial Turbomachinery AB are thanked for their contribution of industrial knowl-

edge.

Finally, I thank my family for their support, and in particular my sister Maren for her help on my manuscript. Last, but not least, I owe my gratitude to Marianne for her patience, support, and self–sacrifice.

Contents

Nomenclature

Latin uppercase

$\mathbf{A}$	State-space model coefficient matrix
$\mathbf{B}$	State-space model coefficient matrix
$\mathbf{C}$	State-space model coefficient matrix
$\mathbf{D}$	State-space model coefficient matrix
F_T	Turbine flow–pressure characteristic
G_Q	Heat release transfer function model
$G_{Q,n}$	Normalized heat release transfer function model
$\mathbf{I}$	Identity matrix
J	Cost function for LQR design
J_s	Square of rotating stall amplitude
$\mathbf{K}$	Innovations state-space model coefficient matrix
$\mathbf{K}_f$	Kalman–filter matrix
K_p	Gain constant for proportional part of the PID controller
$\mathbf{K}_m$	Kalman–filter matrix
$\mathbf{K}_v$	Kalman–filter matrix
$\mathbf{K}_x$	Kalman–filter matrix
$\mathbf{L}$	Feedback law coefficient matrix
$\mathbf{L}_\mathbf{v}$	LQR feedback law matrix
L_t	Length of the primary combustion chamber
M	Window length
N	Number of samples
N_z	Number of element in zero–padded sequence
$\mathbf{P}$	Variance matrix

P_d	Pressure at the downstream pressure sensor in the frequency domain
$\mathbf{Q_1}$	Weighting matrix for LQR design
$\mathbf{Q_{12}}$	Weighting matrix for LQR design
$\mathbf{Q_2}$	Weighting matrix for LQR design
Q_f	Heat released from the flame at the flame holder in the frequency domain
R	Specific gas constant
$\mathbf{R_1}$	Noise covariance matrix
$\mathbf{R_2}$	Noise covariance matrix
$\mathbf{R_{12}}$	Noise covariance matrix
$\widehat{R}_{xx}$	Estimate of the autocorrelation function
$\widehat{R}'_{xx}$	Estimate of the autocorrelation function
$\bar{\bar{R}}_{xx}$	Windowed estimate of the autocorrelation function
$\mathbf{S}$	Matrix
S_u	Laminar burning velocity
$\bar{\bar{S}}_{xx}$	Estimate of the periodogram function
T	Temperature
T_d	Time constant for differential part of the PID controller
T_i	Time constant for integral part of the PID controller
U_f	Velocity at the flame holder in the frequency domain
U_{na}	Non-actuated velocity at the flame holder in the frequency domain
U_l	Velocity of the loudspeaker membrane in the frequency domain
V_l	Voltage over the loudspeaker in the frequency domain
X_d	Discrete Fourier transform of data sequence

$\mathbb{Z}$	Set of integers

Latin lowercase

$a_1 - a_8$	Moore–Greitzer model coefficients
b_1, b_2	Flame model coefficients
c	Averaged speed of sound
c_v	Specific heat
d	Discrete time delay index
e	Internal energy
e_c	Control error
f_n	Normalized frequency
i	Imaginary unit
i_0	Offset value for valve position estimate
i_{pos}	Valve position estimate
j	Summation index
k	Discrete time index
k_c	Combustion model gain
$k_{l1} - k_{l3}$	Loudspeaker coefficients
l	Discrete frequency index
m	Summation index
$\dot{m}_f$	Fuel mass flow
n	State dimension
p	Pressure
p_0	Mean pressure
p_d	Combustion chamber pressure at the downstream pressure sensor
p_{pz}	Number of parameters to be estimated
p_s	Supply pressure in the fuel supply line relative to atmospheric pressure

p_u	Combustion chamber pressure at upstream pressure sensor
p_v	Pressure over the fixed valve in the fuel supply line relative to atmospheric pressure
q	Heat release
q_f	Heat release at the flame location
r	Radial position
s	Laplace operator
t	Time
u	Velocity of gas component
$\mathbf{u}$	Control input in vector form
u_c	Control input
u_f	Velocity at the flame holder
u_l	Velocity of the loudspeaker membrane
u_{na}	Non-actuated velocity at the flame holder
u_{sv}	Input to the servo valve
u_t	Control input
v	Noise process
v_l	Voltage over the loudspeaker
v_{pfm}	Pulse frequency modulated voltage
w	Noise process
x	Position in combustion chamber coordinate system
$\mathbf{x}$	State vector
$\hat{\mathbf{x}}$	Estimated state vector
$\widetilde{\mathbf{x}}$	Estimation error of the state vector
x_d	Position of the downstream pressure sensor
x_f	Position of the flame holder
x_s	Discrete data sequence
y	Output
$\mathbf{y}$	Control output in vector form

$\bar{y}$	Average of output
$\hat{y}$	Predicted output
z	Noise process

Greek uppercase

Δi_L	Current rise over a PFM cycle
Φ	Mass flow through the compressor
Φ_t	Mass flow through the turbine
Ψ_c	Compressor pressure rise
$\mathbf{\Psi}_o$	Observability Gramian
Ψ_p	Plenum pressure
$\mathbf{\Psi}_r$	Reachability Gramian
Ω	Window function

Greek lowercase

α	Weighting parameter for LQR design
β	Weighting parameter for LQR design
γ	Specific heat capacity
ϵ	Residual between model predicted value and measured data
η_v	Variance ratio
κ_f	Prediction fit
κ_v	Variance-accounted-for
ξ	Axial location of the flame front
ρ	Density
ρ_0	Mean density
τ	Integration variable
ω	Angular frequency in rad/s

Abbreviations

CFD	Computational Fluid Dynamics
CVA	Canonical Variate Algorithm
DFT	Discrete Fourier Transform
FAC	Fuel Actuated Combustion chamber
FFT	Fast Fourier Transform
FPE	Final Prediction Error
HCCI	Homogeneous Charge Compression Ignition
IDFT	Inverse Discrete Fourier Transform
IFFT	Inverse Fast Fourier Transform
LQG-LTR	Linear Quadratic Gaussian-Loop Transfer-Recovery
LQR	Linear Quadratic Regulator
MG3	Third–order Moore–Greitzer model
MOESP	Multi-variable Output-Error State sPace
MVV	Mean Valve Voltage
NO_x	Oxides of nitrogen
PAC	Pressure Actuated Combustion chamber
PDE	Partial Differential Equation
PFM	Pulse Frequency Modulated
PID	Proportional-Integral-Differential
PRBS	Pseudo Random Binary Sequence
RTAI	Real–Time Application Interface
SIMO	Single–Input Multiple–Output
SISO	Single–Input Single–Output
STR	Self–Tuning Regulator

1

Introduction

Combustion processes serve as important sources of energy, for both power generation and for transport, ranging from large scale power stations to micro turbines and aeroplane engines. Even though these different applications are quite different in operating conditions and design, their environmental impact has been subject to stringent restrictions. Figure 1.1 illustrates some of the trends of this.

When considering the emissions of oxides of nitrogen (NO_x), the local temperature in the combustion process plays an important role; the NO_x formation rate increases exponentially with the flame temperature [Saravanamuttoo *et al.*, 2001]. Even if the average temperature inside the combustion zone is kept relatively low, local zones with higher temperature (hot–spots) may cause significant NO_x formations. Several design methods focus on uniform combustion to avoid hot–spots. One example of such combustion is the HCCI engine where fuel and air are premixed inside the combustion chamber and charged by compression [Christensen *et al.*, 1998]. Another example is lean, premixed gas–turbine combustion chambers. Aircraft engines have diffusion–flame combustors, where the fuel is sprayed into an air flow, building a flame front near stoichiometric conditions. The near–stoichiometric combustion generates fairly stable flames, but also high temperatures at the flame front leading to high NO_x formations. Premixed, and especially lean premixed, combustion can be an answer to this problem. Here the fuel and air is mixed before the combustion. If the reactants are mixed properly, the fuel–air ratio is uniformly distributed, and hot–spots can be avoided. A disadvantage with lean premixed combustion is that the

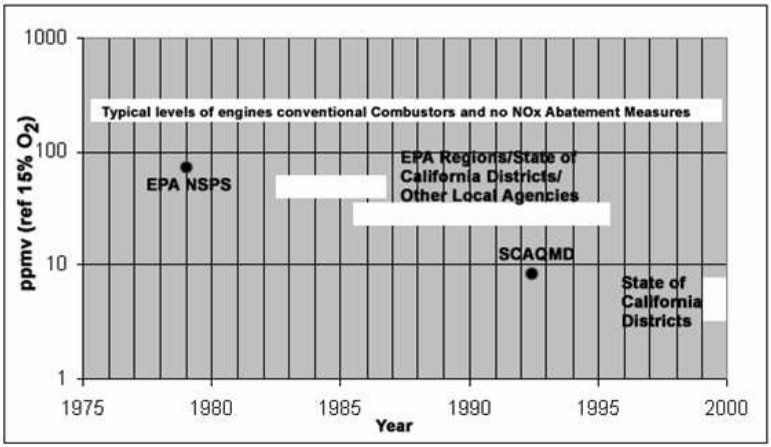

Figure 1.1 Trends in NO_x standards prescribed in the United States for industrial engines [Bahr, 1999].

pressure may enter unstable limit cycle behavior where the amplitude grows until some constant amplitude is reached. This behavior is most undesirable, and can even damage the engine, see [Saravanamuttoo *et al.*, 2001] for a more complete discussion on the different combustion techniques. Active control provides tools to stabilize the unstable combustion processes, thereby allowing lean premixed combustion [Dowling and Morgans, 2005]. Advance in computer software, sensors, actuators, and the understanding of the combustion process has provided tools and know–how to develop active control systems for combustion processes for gas turbines [Zinn, 2005].

This thesis addresses the issue of stabilizing unstable combustion oscillations by testing different control strategies on an atmospheric, lean premixed combustion test rig.

Outline of the Thesis

Chapter 2 summarizes some important results on modeling and control of unstable combustion processes. Other subjects related to gas–turbine dynamics are also briefly mentioned. Chapter 3 describes the experimental setup of the atmospheric lean premixed combustion chamber with sensors, actuators, and computer resources, constructed within the work of this thesis. Chapter 4 describes theoretical and practical issues used to design control systems for the combustion rig described in Chapter 3. The design of an actuator is treated along with methods for model identification and model–based control design. The results of the system identification are listed in Chapter 5. The identified models, along with the methods described in Chapter 4, are used to design controllers, which are tested and documented in Chapter 6. Chapters 7 and 8 discuss the results, state conclusions, and describe relevant further work.

2

Background

2.1 Combustion Instability

Combustion instability was reported in 1859 when Rijke described his experiment with a vertically mounted tube with a flame inside [Rijke, 1859]. His experiment has become a classical laboratory experiment, even for today's research. In 1878 Rayleigh explained the combustion instability by:

"If heat be periodically communicated to, and abstracted from, a mass of air vibrating (for example) in a cylinder bounded by a piston, the effect produced will depend upon the phase of the vibrations at which the transfer of heat takes place. If heat be given to the air at the moment of greatest condensation, or taken from it at the moment of greatest rarefaction, the vibration is encouraged. On the other hand, if heat be given at the moment of greatest rarefaction, or abstracted at the moment of greatest condensation, the vibration is discouraged" [Rayleigh, 1878].

This quotation was accompanied by a more detailed treatment in [Rayleigh, 1877]. The quotation corresponds well with the often used block diagram representation of the combustion process, illustrated by a feedback interconnection between the acoustics of the combustion chamber and the heat release of the flame as illustrated in Fig. 2.1.

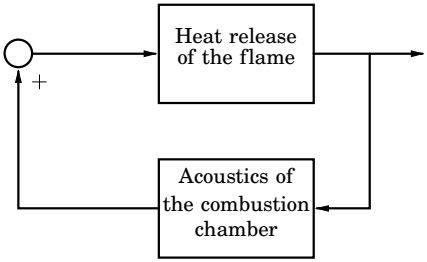

Figure 2.1 Block diagram of interconnection between the combustion chamber acoustics and the heat release of the flame.

The feedback can introduce a local unstable closed–loop system, where amplitudes of the variables grow.

The criterion of Rayleigh states that combustion instabilities occur when the pressure perturbations are in phase with the heat release of the flame. The amplitudes will grow until losses become sufficiently high, and a limit–cycle behavior is reached. If the heat release is in anti–phase with the pressure perturbations the amplitudes will not grow, and no combustion instability will be present. This simple criterion has been an inspiration for many control designs for suppressing combustion instabilities. If either the heat release or the pressure perturbations can be forced to change phase, the criterion of Rayleigh is not fulfilled, and the unstable combustion is stabilized. Dowling and Morgans (2005) describe such various control attempts.

Culick made significant contributions on the modeling of the thermoacoustic instability by including nonlinearities. These nonlinearities bounded the increasing amplitudes of the combustion process variables, resulting in a limit cycle behavior [Culick, 1976a], [Culick, 1976b]. Examples of later work on identifying nonlinear couplings between the pressure perturbations and the heat release are elaborated by Rumsey *et al.* (1998) and Dunstan *et al.* (2001).

Acoustics of the Combustion Chamber

The acoustics are often modeled by formulating the balance equations for mass, moment and energy. A treatment of such balance equations is found in for example [Anderson, 1995].

Heat Release of the Flame

The flame is a complex phenomenon, the modeling of which involves many disciplines such as acoustics, chemistry, fluid dynamics, turbulence, and thermodynamics. It is often impossible to focus on only one of these disciplines, because the interconnections are so strong. Because of the complexity, investigations are often performed numerically by computational fluid dynamics (CFD) techniques. Consult [Poinsot and Veynante, 2001] for a treatment of theoretical and numerical combustion modeling for CFD applications. Such modeling often results in a large number of states, not suitable for on–line evaluation or control design. Low–order models of the flame have been studied in order to derive models of dimensions suitable for control design. Examples hereof are the work of Fleifil *et al.* (1996) and Dowling (1999). A flame model of Dowling (1999) is reprinted here

$$\frac{\partial \xi}{\partial t} = u - S_u \left(1 + \frac{\partial \xi}{\partial r}\right)^{1/2},$$

where ξ, u, and r are the axial location of the flame front with respect to the anchoring point, the component velocity, and the radial position, respectively. The heat release is assumed proportional to the flame–front area [Dowling, 1999].

2.2 Control Methods for Combustion Instabilities

Various strategies have been investigated in order to remove or suppress combustion instabilities when observed in combustion chambers. Traditionally the combustion community distinguishes between two groups of control strategies; passive and active. Passive control strategies rely on fixed solution, unchanged during operation, whereas active control strategies are based on some actuators changing some variable over time.

It is emphasized that the use of the term *passive control* is independent of the definition commonly used within the control community, which is an energy–interpreted property often used in stability evaluation of interconnected systems, as described by, for instance, Khalil

(2002). In this thesis, the term *passive control* is used in the combustion chamber terminology, unless stated differently.

Passive Control Strategies

The first strategies, still used today, focus on changing either the acoustic properties of the combustion chamber or the properties of the flame by redesigning the structure. One example is acoustic dampers such as Helmholtz resonators. Along with many others, these methods are modifications performed during design and are unchanged during operation. Solutions using these methods are often designed *ad hoc* and are only efficient over a limited operating range. Furthermore, a passive control design for a certain combustion chamber cannot be transferred to another design, therefore costly experiments and evaluation must be performed for each design. Saravanamuttoo *et al.* (2001) and Dowling (1999) describe some of the different passive control principles available.

Active Control Strategies

Active control of combustion processes is an active research field, driven by faster actuators and the need for low emission combustion. Many actuator strategies have been studied, including fuel modulation and pressure actuation. The active control results are based on different control strategies, ranging from pure feed–forward control derived by experiments to model–based adaptive control. A comprehensive list of active combustion stabilization results over the last twenty years is presented by Dowling and Morgans (2005).

Active control designs have the advantage over the passive that implementations can, in some cases, be transferred to other combustion chamber designs, reducing the development cost. A significant disadvantage is the reliability of the implementation. In case of failure of the control structure, the whole engine might fail, which is absolutely unacceptable, particularly for aircraft engines.

Neumeier and Zinn (1996) presented successful damping of a gaseous rocket combustor by identifying the unstable modes on–line and apply counter acting fuel modulations with off-line determined phases and amplitudes. The gain and delay of the actuator at the given instability frequency were identified in off-line experiments. In on-line

operation, these parameters were used to generate an actuator signal forcing the heat release to be in anti–phase to the pressure.

Annaswamy *et al.* (2000) reported control results operating a premixed atmospheric combustion process with dominating resonance frequency around 470 Hz. Noise damping of 45 dB was accomplished using LQG-LTR control design and a loudspeaker for pressure actuation.

Recently, Hermann *et al.* (2000) reported successful damping of combustion instabilities in an industrial gas turbine operated for 6000 hours. Each of the 24 burners were equipped with fuel actuation on the pilot, and damping of around 20 dB at the resonance (approximately 145 Hz) was achieved. The control design was based on on–line identification of the resonance frequency and applying an offline–designed phase shifted actuation signal.

A series of interesting results have recently been reported on tests on an atmospheric rig with main resonance at around 200 Hz with 30-39 dB damping of the resonance was obtained using various control designs such as H_∞[Morgans and Dowling, 2005], STR [Riley *et al.*, 2004], and adaptive control [Riley *et al.*, 2003]. The control designs were based on empirical models.

Zinn (2005) and Annaswamy and Ghoniem (2002) describe some of the different active control results.

Actuators

Loudspeakers show satisfactory actuation results in laboratory experiment due to their high frequency response [Dowling and Morgans, 2005]. However, loudspeaker actuation suffer from lack of robustness towards the harsh environment of large scale combustion chambers, and power requirements are difficult to scale to large scale applications [Dowling and Morgans, 2005]. According to Dowling and Morgans (2005), modulation of the chemical energy release by fuel modulation shows an efficient method for actuation of the combustion process. Several implementations of fuel modulations have been reported recently, ranging from on–off car fuel injectors [Langhorne *et al.*, 1990], magnetostrictive actuated valves [Neumeier *et al.*, 1997], spinning valves [Barooah *et al.*, 2003], and piezo valves [Ikame *et al.*, 2005], [Hermann *et al.*, 1996]. Both Dowling and Morgans (2005) and Zinn (2005) state that one of the main challenges facing implementation of active controlled combustion stabilization is satisfactory valve designs.

2.3 Pressure-Flow Coupled Instability

The pressure–flow coupled instabilities are not traditionally related to combustion instabilities, but are treated for completeness.

Surge and rotating stall are severe instabilities occurring due to component interactions in the gas turbine.

Surge

Surge is traditionally treated as a pure compressor phenomenon. If a sudden mass flow drop occurs under low mass flow operation, the pressure at the compressor outlet will reduce. Since the pressure downstream to the compressor does not reduce immediately, the flow reverses direction, and the pressure at the compressor outlet drops further. Meanwhile, the pressure downstream will have fallen sufficiently to ensure a mass flow in the right direction, increasing the pressure rise of the compressor. This cycle will repeat, and a limit cycle behavior will occur in the flow and pressure, see Saravanamuttoo *et al.* (2001) for more discussion on surge in compressors.

Greitzer (1976) formulated a simplified dynamic model of flow in compressors. This model can be used to model the gas turbine set–up illustrated in Fig. 2.2. The model was derived assuming constant temperature throughout the whole system, uniform density in the compressor-plenum pipe, and uniform density and pressure in the plenum, and can be formulated as

$$\begin{aligned} \frac{d\Psi_p}{dt} &= a_1 (\Phi - \Phi_t) \\ \frac{d\Phi}{dt} &= a_2 (\Psi_c - \Psi_p) \quad . \end{aligned}$$

The variables Ψ_p, Ψ_c, Φ, and Φ_t are the plenum pressure, the compressor pressure rise, the mass flow through the compressor, and the mass flow through the turbine, respectively. The coefficients a_1 and a_2 define the dynamics. Actuation strategies such as closed coupled valves, plenum pressure actuators and variable compressor speed has been suggested, see [Gravdahl, 1998] for more details. Surge can be modeled by assuming the static relationship between the compressor flow and pressure rise, and the static relationship between turbine

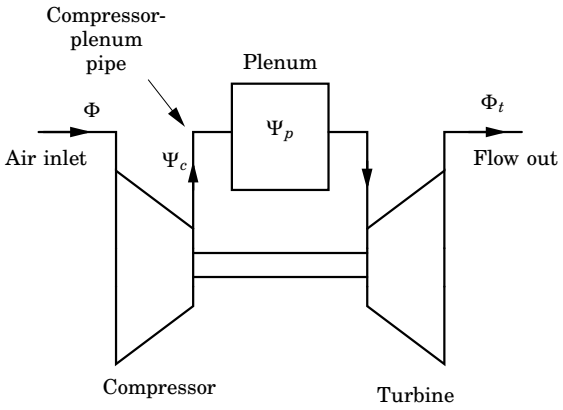

Figure 2.2 Schematic diagram of a gas turbine. The air enters through the air inlet and the pressure is raised by a compressor, where Φ is the mass flow through the compressor and Ψ_c is the pressure over the compressor. The compressor is connected to a plenum by a pipe. The variable Ψ_p is the plenum pressure. The gas leaves the plenum through a turbine, where Φ_t is the mass flow through the turbine. For gas–turbine applications, the compressor and the turbine are often mechanically connected by a shaft.

flow and pressure drop. Often used approximations are polynomials as illustrated in Fig. 2.3 [Greitzer, 1976], [Gravdahl, 1998]. The steady–state operating point is defined by the intersection of the compressor and turbine characteristic. Due to the negative slope of the compressor characteristic to the left of the surge line, operating points to the left of the surge line are unstable, and operation within this region causes severe oscillations in both pressure and flow.

Rotating Stall

Rotating stall is also traditionally treated as a compressor phenomenon caused by breakdown in the compressor channels and is often observed during *off–design operation*[1]. Rotating stall occurs, when the flow through a channel in the compressor brakes down. This increases

[1]Off–design operation relates to operating conditions removed from the design point [Saravanamuttoo *et al.*, 2001]. Examples of such operation conditions are acceleration, idling, and large angles of incidence.

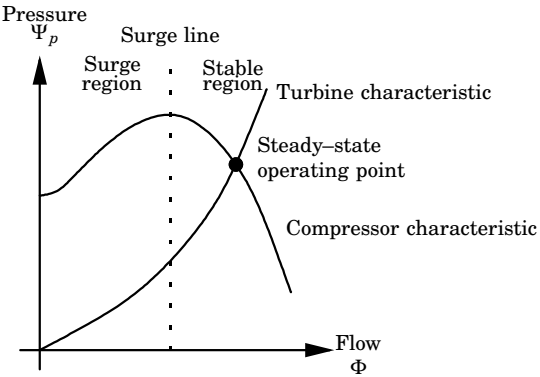

Figure 2.3 Compressor and turbine characteristics. The steady–state operation point is defined by the intersection of the two characteristics. Operation is unstable to the left of the surge line and stable to the right.

the angle of incident for one of the neighbor channels and decreases it for the other neighbor. The channel with increased angle of incident stalls, and changes the angle of attack on the previous stalled channel, which is thereby recovered. The stall moves in this manner from channel to channel, from which the term *rotating stall* origins [Saravanamuttoo *et al.*, 2001]. The effects are vibrations and reduced pressure rise over the compressor, which in worst case requires engine stop to be restored. A general discussion on rotating stall in compressors can be found in, for example, [Saravanamuttoo *et al.*, 2001].

The Greitzer model was expanded by Greitzer and Moore (1986) to include the rotating stall instability, represented by the variable J_s ;

$$\frac{d\Psi_p}{dt} = a_3 \left[\frac{\Phi}{a_7} - \frac{1}{a_7} F_T^{-1}(\Psi_p) \right]$$

$$\frac{d\Phi}{dt} = a_4 \left[-\frac{\Psi_p - a_5}{a_6} + 1 + \frac{3}{2}\left(\frac{\Phi}{a_7} - 1\right)\left(1 - \frac{1}{2}J_s\right) - \frac{1}{2}\left(\frac{\Phi}{a_7} - 1\right)^3 \right]$$

$$\frac{dJ_s}{dt} = a_8 J_s \left[1 - \left(\frac{\Phi}{a_7} - 1\right)^2 - \frac{1}{4}J_s \right] \quad , \; J_s \geq 0$$

where $a_3 \cdots a_8$ are coefficients [Greitzer and Moore, 1986]. This model

is often denoted MG3 (third–order Moore–Greitzer model) in gas turbine control literature.

2.4 Scientific Challenges

Actuator Design

Combustion chambers are harsh environments and implementing actuators is a challenging task. Combustion chamber designs are often time consuming and expensive, and the need of modification of the design due to the implementation of actuator should be kept to an absolute minimum. As Dowling and Morgans (2005) state, fuel modulation holds promising possibilities, even though most actuators here suffer from bandwidth limitations.

Deriving Dynamic Models of the Combustion Process

The combustion process is a complicated phenomena, involving thermodynamics, chemistry and acoustic problems. Models derived to describe the interaction between all these complicated phenomena often result in highly complex and nonlinear models, not suited for on–line computation and feedback control design. Suitable input–output models are therefore more likely to be derived on empirical grounds [Dowling and Morgans, 2005].

Study of a General Structure for Active Combustion Control

Besides the problems of combustion instability, surge, and rotating stall, research is done in the control of emissions, pattern factor, lean blowout, and engine health. To reduce the number of actuators and sensors and to avoid negative interference between these different control systems, research into unifying all these strategies is relevant [Zinn, 2005].

Furthermore such control systems should be robust and capable of ensuring long term operating under harsh engine environment [Zinn, 2005].

3

Experimental Combustion Rig

The test rig designed within the project cannot be compared to industrial combustion chambers in terms of dimensions. However, it was capable of generating the important thermoacoustic instability phenomena in a comparable frequency domain, without the need of cooling or other complications. The scope of this research project has been the active stabilization of thermoacoustic instabilities, and the simple test scenario can serve as a demonstration of what can be achieved with this technology.

The test rig was based on an earlier prototype designed by Mijic and Stödberg (2004).

The test rig consisted of an atmospheric combustion chamber designed for gaseous fuel and self–driven air supply. The gas was supplied from a gas container and could be adjusted through a number of valves. Upstream of the flame holder a loudspeaker was mounted and several sensors were available for data acquisition and feedback. Figure 3.1 illustrates the whole test rig apart from the computer system and Table 3.1 lists the components.

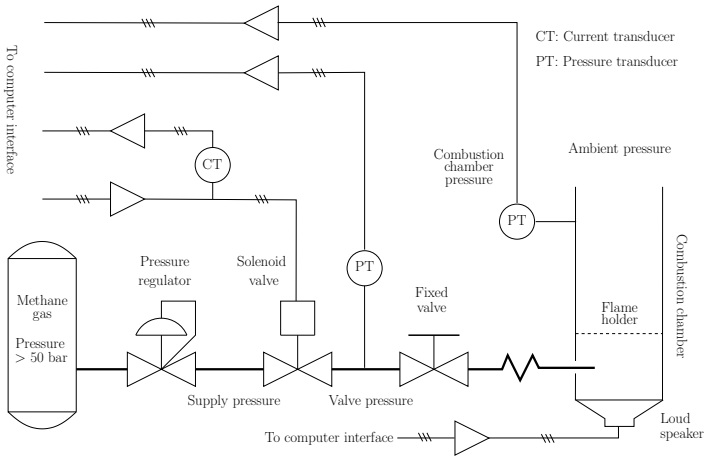

Figure 3.1 Diagram of test rig.

Table 3.1 Components.

Flame holder	∅61 mm metal grid. Grid size: 0.9×0.9 mm.
Pressure regulator	Air Liquide H-REG HBS 240-8-3 H2.
Solenoid valve	Servojet HSV 3000.
Combustion chamber pressure sensors	Capacitor microphone element, www.Elfa.se, article number 30-105-50.
Fuel pressure sensor	Afrisco Euro-Index, DMU01, 0-3 bar.
Loudspeaker	www.Elfa.se, 10 W, article number 30-375-04.
Loudspeaker amplifier	Kemo universal amplifier, 12 W, article number M032.

3.1 Combustion Chamber

The combustion chamber was a lean premixed gas combustor. It consisted of a primary and a secondary chamber. Figure 3.2 illustrates a

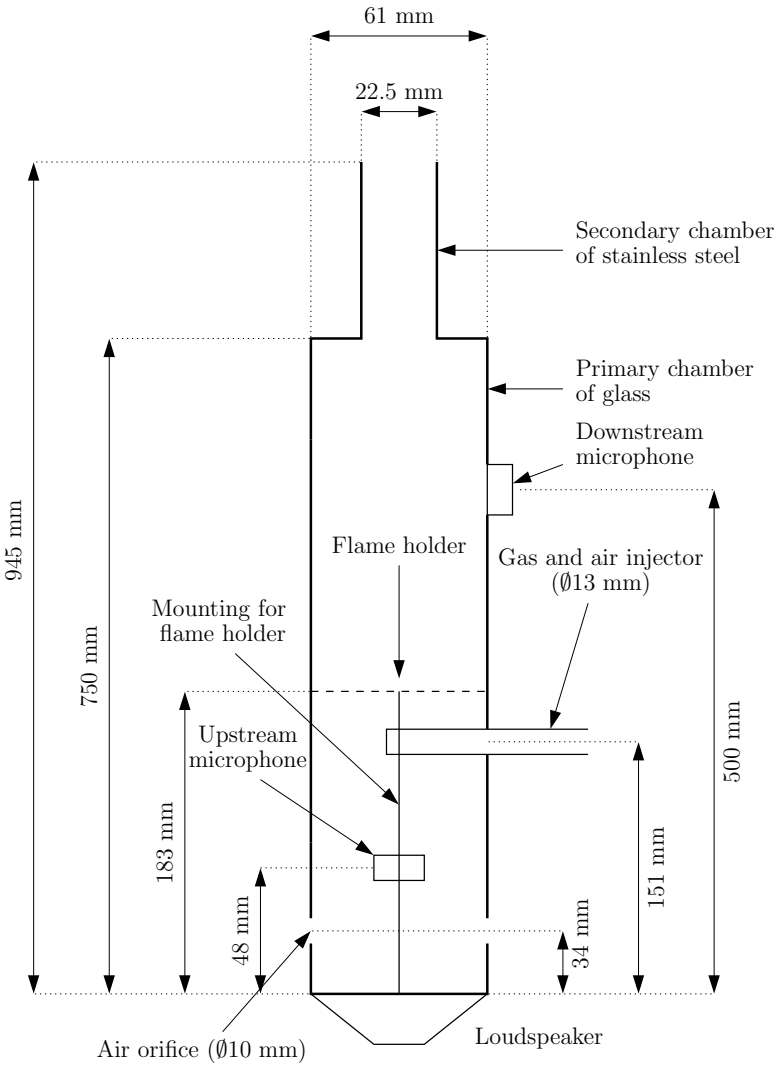

Figure 3.2 Schematic drawing of the combustion chamber.

schematic drawing of the combustion chamber.

The primary chamber was a vertical cylindrical glass tube. A loudspeaker was mounted in the bottom, fitting the entire transversal section. The gas was injected through a Bunsen burner over which a flame holder was mounted. The flame holder covered the full combustion area. Air was driven into the chamber by the drag from the rising hot air through four air orifices in the bottom of the chamber and through the Bunsen burner. Since the fuel entered with vertical velocity sufficient turbulence for mixing of air and fuel was obtained.

The secondary combustion chamber was a smaller tube of stainless steel mounted on top of the primary chamber (Fig. 3.2). Its main purpose was to modify the acoustic impedance, and thereby the acoustic properties of the entire chamber. The secondary chamber was removable allowing the primary chamber to operate with a fully open top.

Methane gas was used for fuel in all experiments presented in this thesis.

The dominant resonance frequency of the primary combustion chamber was approximately 275 Hz. Including the the secondary chamber, the resonance frequency of the combustion chamber was approximately 185 Hz. The wavelength of the resonance frequency of the primary combustion chamber corresponded to twice the length of the primary combustor.

3.2 Fuel Supply

The fuel supply line consisted of three flow regulating devices and appropriate gas lines. The gas was supplied from a container and regulated from the container pressure (> 50 bar) to a lower pressure, denoted the supply pressure p_s. This pressure remained constant during experiments due to the pressure regulator. For computer regulation of the fuel flow two valves followed; one was fixed and one was adjustable, the former being a solenoid valve actuated by a voltage signal. Assuming the downstream pressure remained constant, the pressure over the two valves was assumed constant as well (assuming the pressure drop over the final supply line was negligible). Opening and closing of the solenoid valve resulted in decreasing and increasing pressure drop over the solenoid valve, respectively. Since the pressure over the two valves

remained constant, the pressure drop over the fixed valve increased as the pressure drop over the solenoid valve decreased and *vice versa*. The gas flow (assumed to be constant over the whole supply line) thereby increased and deceased as the solenoid valve opens and closed, assuming that the flow through the fixed valve was proportional to the square root of the pressure drop over the valve.

A 740 mm supply line connected the fixed valve with the combustor. Depending on operating conditions the fuel flow was in the range of 0-3 l/min.

3.3 Pressure Actuator

A loudspeaker was mounted in the bottom of the combustion chamber, driven by an amplifier.

3.4 Computer Resources

The data system for data acquisition and control consisted of:

- A 800 MHz Pentium® PC.
- Linux Redhat 9 operating system.
- An Advantech 1711 digital/analog interface with the sampling frequency of 10 kHz.
- A RTAI real–time system with control and calibration implementation.
- Appropriate software for data logging and administration of the control algorithms.

To ensure appropriate real-time performance, the control software was implemented in the kernel space of the Linux/RTAI environment. Figure 3.3 illustrates the software and hardware interaction. Information could only be exchanged along the indicated arrows, when the kernel module allowed. The real–time system ensured that all processes in the kernel space were executed at specific sampling times. Only the surplus of computational power could be used by the user interface

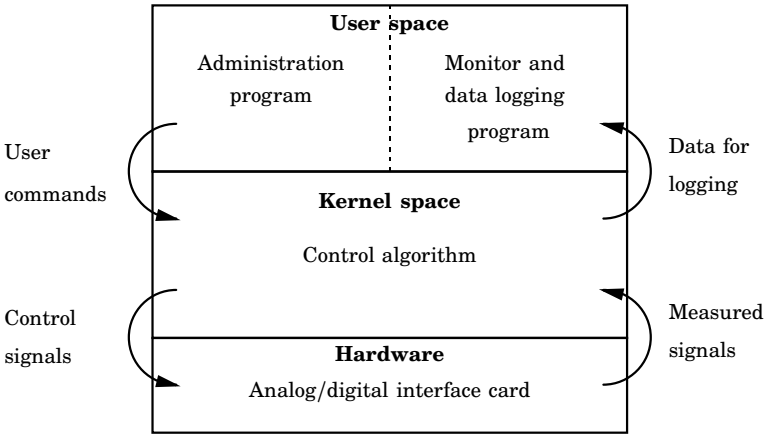

Figure 3.3 Software and hardware interaction in the Linux/RTAI environment.

applications, which were not as time critical. The kernel space also handled the interaction with the analog/digital interface card by requesting measurements and physical port voltage values.

The implementation allowed feedback from three types of measurements; the solenoid valve current, the valve pressure, and the combustion chamber pressure (all analog measurements), and for logging all relevant signals. The signal to the solenoid valve and the loudspeaker were affected by digital and analog ports, respectively.

3.5 Electronics

Valve Driver and Current Measurement Circuit

The digital signal from the analog/digital interface card was current amplified in order to drive the driver circuit. A MOSFET transistor allowed for switching of the voltage over the solenoid valve between 0 V or 23.3 V. A high power resistor inserted in series with the solenoid valve allowed current measurement. This signal was amplified with

an operational amplifier circuit and filtered (see the circuit diagram in App. B.1 on page 102). The signal was further amplified by an amplifier (see the comment in App. B.3).

Valve Pressure Measurement Equipment

The pressure between the solenoid and the fixed valve relative to atmospheric pressure was measured with a pressure transducer. It reported the pressure in terms of a current signal, which was converted into a voltage signal and amplified by an amplifier (see the comment in App. B.3).

Combustion Chamber Pressure Measurement

Two pressure transducers were implemented on the test rig. One was mounted upstream of the flame holder, where the temperature was relatively low and one downstream of the flame holder, where the temperature was relatively high. Due to the high temperature downstream of the combustion zone, the downstream pressure transducer was not mounted when the secondary chamber was included. Both pressure transducers were capacitor microphone elements (see the circuit diagram in App. B.2 on page 103). The signal was amplified by an amplifier (see comment in App. B.3).

4

Methods

Four measurements were available for feedback; the solenoid valve current, the valve pressure, and the combustion chamber pressure at the up-and downstream pressure sensor. The two first measurements were related to the fuel supply only. Since the solenoid valve had an on/off characteristic, a local feedback loop was designed to control the solenoid valve position. Using this actuator design, the two inputs to the combustion chamber were the loudspeaker signal and a reference for the solenoid valve position. The outputs were then the actual solenoid valve position (or an estimate thereof), the valve pressure, and the combustion chamber pressure from the pressure sensors.

A control strategy based on pressure actuation is illustrated in Fig. 4.1. This method fixated the fuel supply, and the measurements of solenoid valve position and the valve pressure were irrelevant for pressure stabilization purpose. Excluding the secondary combustion chamber, the downstream pressure sensor was applicable. This system was denoted the pressure actuated combustion chamber (PAC). A second method was based on fuel modulation, and here all available measurements could hold relevant information, which is illustrated in Fig. 4.2. The fuel actuator was tested in combination with the secondary combustion chamber, which excluded the downstream pressure sensor due to the increased temperatures downstream. This system was denoted the fuel actuated combustion chamber (FAC).

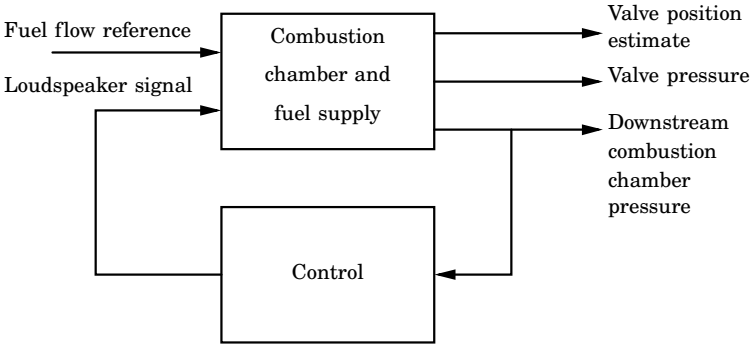

Figure 4.1 Block diagram for the control structure based on pressure actuation (PAC).

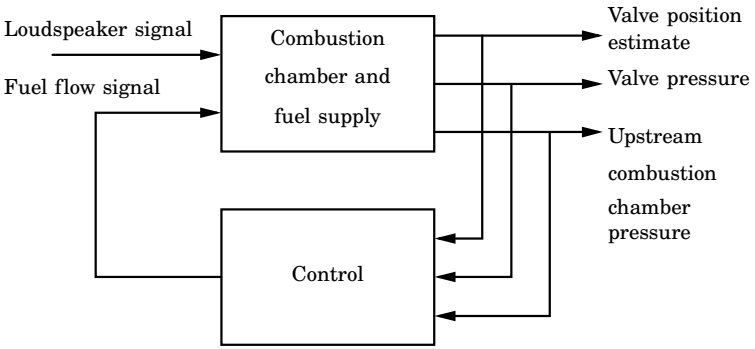

Figure 4.2 Block diagram for the control structure based on fast fuel–actuation (FAC).

4.1 Fast Fuel–Actuation Implementation

Solenoid valves are often used for flow control because of their relatively low price, their simple design (high reliability), and fast response. They are often used for switching applications where the flow is either blocked or allowed to pass. Many applications require a more proportional or graded behavior, where different levels of flow can be

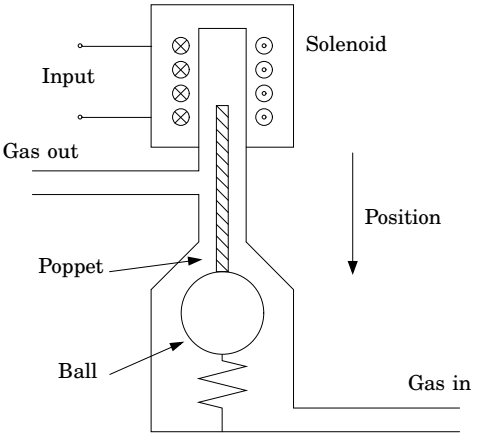

Figure 4.3 A solenoid valve.

obtained. Such valves exist today, driven by stepper motors or other mechanical devices, but they are complicated in design and expensive compared to solenoid valves. Converting the solenoid valve to behave in a proportional manner, seems therefore attractive and was investigated within the research presented in this thesis.

To keep costs down, it was preferable to do the conversion only adding electronic components, which had a low production price, omitting expensive redesign of the valve itself. One option for conversion was to use feedback, which still holds great variety of solutions. Lim *et al.* (1994) reported successful position control of a general purpose solenoid, using measurements of electric signals from the solenoid and some internal position, requiring redesign of the valve in many cases. Rahman *et al.* (1996) reported successful proportional control of a solenoid using only measurements of electric signals, but based on a complicated implementation.

Figure 4.3 illustrates the design principle of the investigated solenoid valve. An electric signal generated a magnetic field, affecting a force on the poppet, causing it to move. A spring forced the poppet and the ball back when the magnetic field was removed. Depending on the position of the ball and poppet, gas was allowed to pass. To

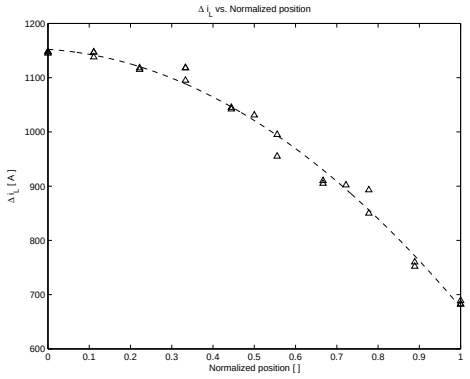

Figure 4.4 Δi_L as function of position. The position is normalized so that zero and one correspond to closed and open position, respectively.

control the flow, it was desirable to control the position of the ball and poppet, which was not a trivial task, since no means for direct position measurements were available. However, the electric properties of the solenoid were influenced by the poppet through the inductance, and intelligent design of voltage actuation and current measurement could give an indication of the position. This principle was studied by Rahman *et al.* (1996). The implementation required that the time derivative of the current was measured. Furthermore, it required a position measurement to generate a lookup table prior to operation, which in many cases is not desirable.

The following describes a principle of using only a simple current measurement for position control of the solenoid valve for flow control, without the need of direct position measurement for calibration.

Servo Valve Design and Induction Based Estimation

To be able to extract the position information, a detailed model of the solenoid was desirable. However, the couplings between electric, magnetic, and mechanical dynamics were too complicated, where factors like friction and temperature dependence added to the complexity. Cheung *et al.* (1993) derived a model, which required measurement of magnetic flux and the possibility to mechanically control the poppet

in order to identify parameters. Also, high parameter sensitivity was reported in part of the operating region. Considering these modeling problems, a more empirical approach was taken.

Applying a pulse frequency modulated (PFM) voltage signal over the solenoid ensured a continuing series of first–order step responses of the current. The current increment over the time duration of a pulse depended on the inductance and, therefore, on the poppet position. This current increment was denoted Δi_L. Recalling the control objective (flow control), knowing the exact position was not absolutely necessary, since complicated calibration of the flow was still required. Figure 4.4 indicates that Δi_L was strictly monotone with respect to the poppet position, so a secondary control objective was chosen to be the control of Δi_L and not the control of the poppet position. To obtain a signal, strictly increasing with poppet position and more flexible to implementation, the estimator signal was defined as

$$i_{pos} \quad = \quad i_0 - \Delta i_L \ ,$$

where i_0 was a positive offset calibration constant, and the subscript *pos* indicates that the signal was strictly increasing with respect to the poppet position. The input to the pulse modulator was obtained from a proportional controller, and the reference u_{sv} was given with respect to the desired i_{pos}. The pulse modulator was implemented, as illustrated in Fig. 4.5, with a pulse duration of 0.4 ms, with an opportunity for nine different cycle times between 0.6 - 1.4 ms. The flow range for this setup was approximately 0.5-1 l/min.

The valve pressure sensor inserted between the solenoid valve and the fixed valve indicated flow (since the flow through the valve was approximately proportional to the square of the pressure over the fixed valve). The design is illustrated in Fig. 4.6.

This setup was designated the servo valve[1], and could be regarded as one integrated dynamic system, with the position estimate reference

[1]It should be noted that the term *servo valve* often refers to a specific implementation by certain valve manufacturers. However, the definition in [Merriam-Webster, 1987] allows a more general use of the term. Webster's Dictionary: *"[servo- (as in servomotor) +mechanism](1944): an automatic device for controlling large amounts of power by means of very small amounts of power and automatically correcting the performance of a mechanism"*

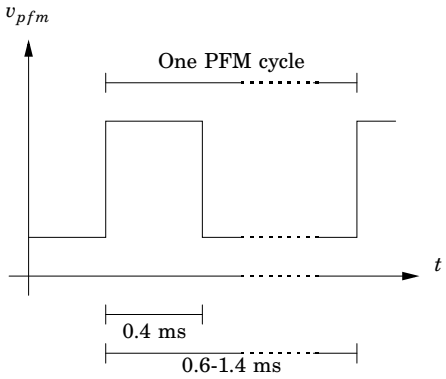

Figure 4.5 Pulse frequency modulated voltage signal. The variable v_{pfm} is the PFM voltage applied over the solenoid–resister network.

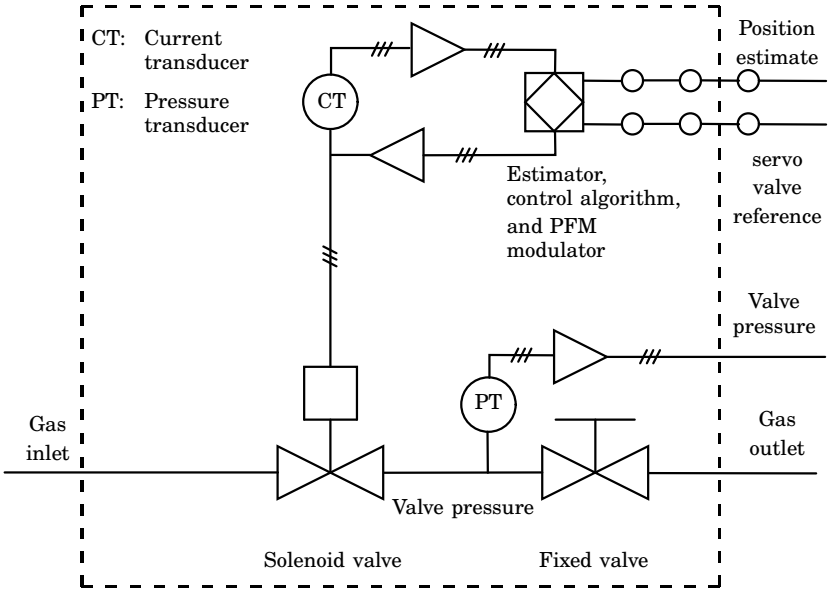

Figure 4.6 Diagram of servo valve implementation.

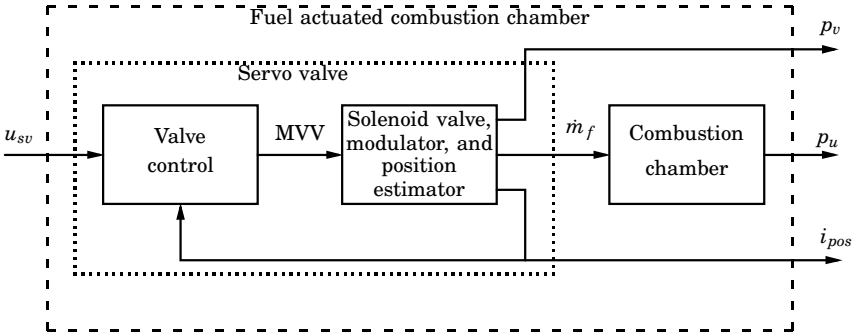

Figure 4.7 Block diagram representation of the fuel actuated combustion chamber. The dashed line indicates the components of the fuel actuated combustion chamber. The dotted line indicates the components of the servo valve. The variables u_{sv}, v_l, MVV, $\dot{m}_f$, p_v, p_u, and i_{pos} are the input to the servo valve, the voltage over the loudspeaker, the mean valve voltage, the fuel mass flow, the pressure over the fixed valve in the fuel supply line relative to atmospheric pressure, the combustion chamber pressure at upstream pressure sensor, and the valve position estimate, respectively.

u_{sv} as input and the position estimate i_{pos}, the valve pressure, and the gas flow as outputs. This is illustrated by the dotted box in Fig. 4.7. Combined with the primary and secondary combustion chamber, the servo valve formed the fuel actuated combustion chamber .

4.2 Identification of Dynamics

Identification of dominating dynamics of the system to be controlled, is a requirement for successful control design. Several methods exist to identify such dynamics, of which two are treated here; analytical modeling and system identification.

The description of system identification methods presented here, follows that of Johansson (1993).

State–Space Model Identification

A state–space model is a time domain representation for a system

of any order, number of inputs, and number of outputs. The discrete version has the form

$$\begin{aligned} \mathbf{x}(k+1) &= \mathbf{A}\,\mathbf{x}(k) + \mathbf{B}\,\mathbf{u}(k) + v(k) \\ \mathbf{y}(k) &= \mathbf{C}\,\mathbf{x}(k) + \mathbf{D}\,\mathbf{u}(k) + z(k) \ , \end{aligned} \tag{4.1}$$

where the variables $\mathbf{x}(k)$, $\mathbf{u}(k)$, $\mathbf{y}(k)$, and k are the state vector, the input vector, the output vector, and the time index, respectively. $\mathbf{A}$, $\mathbf{B}$, $\mathbf{C}$, and $\mathbf{D}$ are constant matrices. The variables $v(k)$ and $z(k)$ are the process noise and measurement noise, respectively. Both noise variables are assumed to be zero–mean Gaussian white noise process, uncorrelated with any other input.

A number of methods have been derived to approximate state–space models from data, for which some do not require dedicated experiments (only that the input assures sufficient persistency of excitation). Such methods require less time to conduct experiments, but require often higher computer resources. Often experiments are more costly than computer resources, and single–experiment methods are preferred over multi–experiment methods.

Several of the subspace–based methods include estimation of the noise contribution in the form of an innovations model

$$\begin{aligned} \mathbf{x}(k+1) &= \mathbf{A}\,\mathbf{x}(k) + \mathbf{B}\,\mathbf{u}(k) + \mathbf{K}\,w(k) \\ \mathbf{y}(k) &= \mathbf{C}\,\mathbf{x}(k) + \mathbf{D}\,\mathbf{u}(k) + w(k) \ , \end{aligned} \tag{4.2}$$

where $\mathbf{K}$ is a constant matrix and the innovation variable $w(k)$ is a zero-mean white noise stochastic process, independent of the other variables.

Two implementations of subspace–based method were used:

- The MOESP method (Multi-variable Output-Error State sPace) presented by Verhaegen (1994). A MOESP algorithm is implemented for Matlab® in the SMI Toolbox, version 1.0 [Haverkamp and Verhaegen, 1997]
- The CVA method (Canonical Variate Algorithm) presented by for instance Larimore (1983), and van Overschee and de Moor (1996). A CVA algorithm is implemented in the Matlab® System Identification Toolbox®, version 6.1.1 [Ljung, 2005].

Model Validation

The comparison of the model–predicted outputs to the measured outputs yields a method to validate an identified model. The two indices used were the prediction fit and the variance-accounted-for:

$$\begin{aligned} \kappa_f &= 100 \left(1 - \frac{\|\hat{y} - y\|}{\|y - \bar{y}\|}\right) \\ \kappa_v &= 100 \left(1 - \frac{\mathrm{var}\,(y - \hat{y})}{\mathrm{var}\,(y)}\right) \quad . \end{aligned}$$

Model Order Determination for State–Space Model

The first problem of the model identification was to estimate the model order. Several methods to extract this information from input–output data exists, and the following two were used:

- The number of nonzero (or above some small limit) **singular values** of certain data–based matrix could be interpreted as an estimate of the system order, see [Verhaegen, 1994] or [van Overschee and de Moor, 1996] for further details. Tools to derive the singular values are implemented in the SMI Toolbox for Matlab®. The limit, above which the singular values were assumed significant, was obtained by engineering judgment.
- The **Akaike final prediction error** was a quality index used for validation and model order determination, given by

$$\mathrm{FPE}(p_{pz}) = \frac{N + p_{pz}}{N - p_{pz}} \frac{1}{N} \sum_{j=1}^{N} \epsilon_j^2 \ ,$$

  where p_{pz} was the number of parameters to be estimated and the variable ϵ_j was the residual between the model predicted output and the measured output at time index j. The FPE was originally developed to assist the estimation of regression models which require a minimum number of parameters to represent the model. The identified state–space representation could have a higher number of parameters than the equivalent regression model, and this number of parameters was handled by the specific model identification algorithms. It should be noted that for large

data sets, the influence of a faulty estimate of p_{pz} vanished, since $(N + p_{pz})/(N - p_{pz}) \to 1$ as $N \to \infty$.

The FPE was based on model identification by the CVA method in this thesis.

Balanced Model Reduction

Balanced model reduction was established in the early eighties by Moore (1981), Pernebo and Silverman (1982), and others. The method was based on balancing of the input energy required to obtain a certain state, and the state energy required, for $\mathbf{u} = 0$, to obtain a specified output energy for a state–space model.

The balanced model reduction method is implemented in the Matlab® Control System Toolbox®, version 6.2 [MathWorks, 2005].

Identification of Servo Valve Dynamics

System identification was used in the evaluation of the servo valve design. One of the most important properties to estimate was the time delay, which was estimated from the identified models.

A pseudo random binary sequence (PRBS) excitation signal was applied to the servo valve, and subspace–based identification was applied. The PRBS spread the main part of the signal energy over the frequency range 0-1000 Hz. The position estimate and the valve pressure were measured as outputs.

Identification of PAC Dynamics

The primary combustion chamber had relatively simple acoustic properties, and the modeling could therefore be done analytically by stating balance equations, boundary equation, etc. The purpose of the model was to describe the input–output relationship between the loudspeaker action and the measured pressure in the combustion chamber. Modeling of other factors such as flame shape, chemical reactions, and heat loss were therefore regarded to be of secondary importance, meaning that detailed modeling of them was not necessary, when only their effect of the input–output relationship was captured.

Model 1—PAC Model

The following modeling was inspired by Anderson (1995), Egeland and Gravdahl (2002), and Fleifil *et al.* (1998).

To simplify the modeling, it was assumed that the primary combustion chamber was completely uniform in transversal direction, and it was therefore only described in one space dimension along the flow direction. Additional assumptions were made to simplify calculations:

- Inviscid flow;
- The mean flow was negligible;
- Perfect gas ($p = \rho RT$);
- Ideal gas ($R/c_v = \gamma - 1$);
- Constant specific heat ($e = c_v T$);
- Isentropic conditions ($c^2 = \gamma p_0/\rho_0$);
- The kinetic energy was negligible;
- All the external forces were negligible;
- The influence of the dynamics of the chemical reactions was negligible;
- The flame front was infinitesimally thin.

From the above mentioned assumptions, the mass, energy, and continuity equations were reduced to the linearized balance equations:

$$\rho_0 \frac{\partial u}{\partial t} + \frac{\partial p}{\partial x} = 0 \tag{4.3}$$

$$\frac{\partial p}{\partial t} + \gamma p_0 \frac{\partial u}{\partial x} = -(\gamma - 1)q \ , \tag{4.4}$$

where the variable x was the position along the combustion chamber. The position $x = 0$ was the bottom of the combustion chamber, and $x = L_t$ was the top. The variables $u(t,x)$, $p(t,x)$, and $q(t,x)$ were the velocity, the pressure, and the heat release, respectively. The constants γ, p_0, and ρ_0 were the specific heat capacity, the mean pressure, and the mean density, respectively.

Following Fleifil *et al.* (1998), the acoustic impedance of the loudspeaker was neglected, resulting in the boundary pressure conditions

$$p(t,0) = p(t,L_t) = 0.$$

Because the flame was assumed to be infinitesimally thin, the heat release was zero at all locations except at the flame holder. According to [Annaswamy *et al.*, 1997] the flame could be described by a first order low–pass filter on the form

$$Q_f(s) = \frac{b_1}{s + b_2} U_f(s) \ ,$$

where $U_f(s)$ was the velocity at the flame holder, and the constants b_1 and b_2 were flame model coefficients. Assuming that the time constant of the flame was much smaller than the observed dominating resonance frequency, the flame model was further reduced to

$$Q_f(s) = \frac{b_1}{b_2} U_f(s) \ ,$$

which yielded a static relationship between the velocity at the flame location and the heat release.

Since the flame front was considered to be infinitesimally thin, there existed a discontinuity in the heat release at the flame holder position. The non–actuated velocity $u_{na}(t)$ was here approximated by the average of the velocity infinitesimally close to the flame holder from both sides

$$u_{na}(t) = \frac{u(t, x_f^-) + u(t, x_f^+)}{2},$$

where x_f was the location of the flame holder, and $u(t, x_f^-)$ and $u(t, x_f^+)$ were the velocities infinitesimally close to $u(t, x_f)$ upstream and downstream, respectively.

By temporal Laplace transformation of the PDEs and solving for the spatial variable, in order to respect the boundary equation, the non–actuated velocity at the flame holder and the pressure at the

downstream pressure sensor were given by

$$\begin{aligned} U_{na}(s) &= -\frac{\gamma-1}{2\gamma p_0}\frac{1}{\cosh\left(\frac{s\,L_t}{2\,c}\right)}\,Q_f(s) \\ P_d(s) &= \frac{\gamma-1}{c}\frac{\sinh\left(\frac{s\,L_t}{3\,c}\right)\sinh\left(\frac{s\,L_t}{4\,c}\right)}{\sinh\left(\frac{s\,L_t}{c}\right)}\,Q_f(s)\ . \end{aligned} \qquad (4.5)$$

The constant $c^2 = \gamma p_0/\rho_0$ was the square of the speed of sound, and s was the Laplace operator. The variables $U_{na}(s)$, $P_d(s)$, and $Q_f(s)$ were the Laplace transforms of the velocity at the flame holder, the pressure at the downstream pressure sensor, and the heat release of the flame at the flame holder, respectively.

Figure 4.8 illustrates the feedback interconnection between acoustic properties and the flame dynamic of the combustion setup. The heat release of the flame depended on the local velocity at the flame zone. This velocity was dependent on the heat release, and a possible unstable feedback loop existed. The loudspeaker contributed with two effects; one direct and the other indirect. The direct effect related to the membrane acceleration, generating a pressure contribution in the combustion chamber. The indirect effect was the membrane velocity, which affected the velocity through out the whole chamber, and thereby affected the flame, generating a changed pressure field. According to Fleifil *et al.* (1998), the direct effect could be neglected for an end–mounted loudspeaker, and only the indirect effect was taken into account.

The loudspeaker was modeled using voltage and force balances, and yielded the model

$$U_l(s) = k_{l1}\frac{s}{s^2 + k_{l2}\,s + k_{l3}}V_l(s),$$

where the constants $k_{l1}\ldots k_{l3}$ were positive loudspeaker coefficients, and V_l was the voltage over the loudspeaker in the frequency domain.

In order to obtain a finite–order model, approximations were imposed. An example of such approximation is given here, and later used for control design.

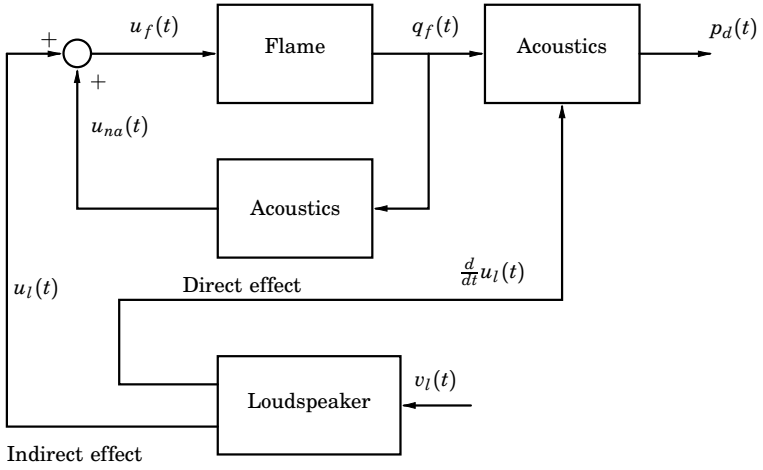

Figure 4.8 Block diagram of the pressure actuated combustion chamber. The variables u_l, u_{na}, u_f, q_f, v_l, and p_d are the velocity of the loudspeaker membrane, the non-actuated velocity at the flame holder, the velocity at the flame holder, the heat release at the flame location, the voltage over the loudspeaker, and the combustion chamber pressure at the downstream pressure sensor, respectively.

EXAMPLE 4.1
By restricting the model to consist of one pair of poles, the following assumption could be suggested

$$2\gamma p_0 = \frac{b_1}{b_2}(\gamma - 1) \ . \tag{4.6}$$

This assumption resulted in heat release dynamics with poles on the imaginary axis, which could be interpreted as the resonance frequencies observed in the experiments, see page 86 for further discussion of this assumption.

The relationship between the heat release and the velocity at the

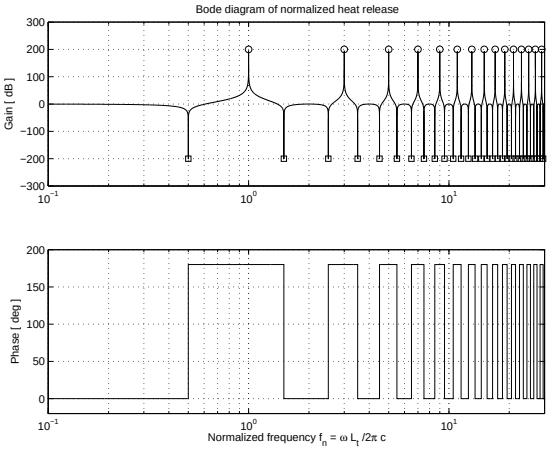

Figure 4.9 Bode diagram of combustion chamber model in Eq. (4.7). The frequency is normalized with respect to the first resonance frequency such that $f_n = \omega L_t/2\pi c$. The transfer function is normalized with respect to the flame flame model parameters, such that $G_{Q,n}(s) = 2G_Q(s)\, b_2/b_1$. The circles and squares indicate infinity (due to singularities) and zero (due to zeros), respectively.

flame holder was then described by

$$Q_f(s) \quad = \quad G_Q(s)U_l(s) = \frac{b_1}{b_2}\,\frac{\cosh\left(\dfrac{s\,L_t}{2c}\right)}{2\cosh^2\left(\dfrac{s\,L_t}{4c}\right)}U_l(s) \quad . \qquad (4.7)$$

Both Eq. (4.5) and (4.7) had infinitely many zeros and poles on the imaginary axis. A normalized Bode diagram of $G_Q(s)$ is illustrated in Fig. 4.9.

The model poles of interest for control design were those also observed in experiments. The transfer function described in Eq. (4.5) had a zero in $\omega = 0$ and low–frequency poles in $\omega = \pi\, c/L_t$ and $\omega = 2\pi\, c/L_t$. Among the low–frequency poles, $\omega = \pi c/L_t$ corresponded to the observed dominating resonance frequency. The heat

release described by Eq. (4.7) had low–frequency zeros in $\omega = \pi\, c/L_t$ and $\omega = 3\pi\, c/L_t$, and low–frequency double poles in $\omega = 2\pi\, c/L_t$. The transfer function from the loudspeaker pressure to the upstream pressure sensor included a pole-zero cancellation at the dominating resonance frequency due to the zero at $\omega = \pi\, c/L_t$. This pole-zero cancellation was present only if the location of loudspeaker, the flame holder, and the pressure sensor were exactly as assumed, and any small deviation would revoke the cancellation. It was therefore assumed that such pole-zero cancellation was not present, and a pole pair existed at the locations $s = \pm i\,\pi\, c/L_t$. The system had an infinite number of poles and zeros, and it made sense to reduce it for control design. Experimental observations indicated that the dominating resonance frequency $\omega = \pi c/L_t$ was absolutely dominant. A simple method to reduce the model order from infinity to a low–order model suitable for control design, was to include the two resonance poles and any poles and zeros of lower frequency in the model. This resulted in the relationship

$$P_d(s) \quad = \quad k_c \, \frac{s}{s^2 + \left(\dfrac{c}{2L_t}\right)^2} \, U_l(s)$$

where the constant k_c was the combustion model gain. Combined with the loudspeaker model, the pressure actuated combustion chamber model became

$$P_d(s) \quad = \quad k_c \, k_{l1} \, \frac{s^2}{\left(s^2 + \left(\dfrac{c}{2L_t}\right)^2\right)\left(s^2 + k_{l2}\, s + k_{l3}\right)} \, V_l(s) \qquad (4.8)$$

□

Identification of FAC Dynamics

The dynamics of the fuel actuated combustion chamber were investigated by means of system identification, due to the non-trivial acoustic properties, introduced by the secondary combustion chamber. Models were estimated using both the CVA and the MOESP method. The implemented excitation signal focused the energy around the relevant

frequencies (0-1000 Hz). It was generated as a PRBS with 2.5 kHz update frequency.

4.3 Control Methods

Phase Shift Control

Phase shift is an intuitive control method used for oscillatory systems. If an unwanted oscillation with one unique stationary and well defined frequency is observed, the system is actuated in a manner that cancels the unwanted oscillations. For example, in the design of noise protection equipment, the noise can be reduced by means of an internal loudspeaker generating sound waves, which are 180°phase shifted from the noise.

This method does not require a dynamical model or profound control design knowledge—only the knowledge of the unwanted frequency and means to affect the process. On the other hand, because of the lack of a model, it is hard to prove stability. Also, this method is sensitive to changes in the system parameters.

The use of phase shift based control for combustion applications was reported by [Ikame *et al.*, 2005].

PID Control

The PID controller has the advantage of being able to be tuned by hand and engineering intuition, and modern off-the-shelf controllers include opportunities for self tuning [Åström and Hägglund, 2005].

The PID controller consists of proportional, integral, and derivative contributions, expressed by

$$u_c(t) = K_p\, e_c(t) + \frac{K_p}{T_i} \int_0^t e_c(\tau)\, d\tau + K_p T_d \frac{de_c(t)}{dt} \ ,$$

where the variable $u_c(t)$ is the control signal and $e_c(t)$ denotes the error between the measured variable and its reference. This formulation is not well suited for implementation, and modification on both the integral and derivative part are often included to avoid integrator windup, and numeric overflow with fast reference changes.

More profound discussions of the PID controller can be found in numerous textbooks, such as [Åström and Hägglund, 2005], [Franklin *et al.*, 1994], and [Haugen, 1994]. PID control of combustion systems was reported by for example Prakash *et al.* (2005).

Loop Shaping

Loop–shaping design is a classical control design method, where the loop–transfer function[2] is manipulated by control design to obtain a desired shape. The term *loop shaping* is taken from [Skogestad and Postlethwaite, 1996], which also gives an introduction to the method. Many other textbooks treat elements of the loop–shaping, and one of such examples is [Franklin *et al.*, 1994]. Some commonly used elements in loop–shaping design are listed in the following.

Notch filters are used to damp the influence of oscillations. The notch filter is a narrow–band rejection filter which filters out any frequency contribution around the resonance frequency from the error signal, and thereby avoids excitation of the resonance. This has the desired effect, when the loop transfer–function is evaluated, but it has an unwanted effect, when the noise is taken into account. If the noise has a contribution around the resonance frequency (and the notch filter reject band), information thereof will be filtered by the notch filter, and will therefore not be compensated for by the controller.

The use of notch filer based control for combustion applications is, for instance, reported by Morgans and Dowling (2005).

Lead and lag Networks are first order compensation filters used to shape phase of the loop transfer–function. Lead compensators increase the phase at a chosen frequency by up to 90°. The lead network also amplifies frequencies above the chosen frequency more than frequencies below. The lag network has high amplification at low frequencies, but a lower amplification at higher frequencies. The phase is lag decreased up to 90°around a chosen frequency.

Treatment of lead and lag networks can be found in for example [Franklin *et al.*, 1994].

[2]The loop transfer–function is the series connection of the control and process transfer functions.

LQR

A linear quadratic regulator (LQR) for the system of Eq. (4.1) is designed by minimizing a quadratic loss function, where the perturbation of the states and inputs can be penalized with respect to each other. The loss function is defined as

$$J(\mathbf{u}) = \sum_{k=0}^{N-1} \mathbf{x}^T(k)\,\mathbf{Q_1}\,\mathbf{x}^T(k) + \mathbf{u}^T(k)\,\mathbf{Q_2}\,\mathbf{u}(k) + 2\,\mathbf{x}^T(k)\,\mathbf{Q_{12}}\,\mathbf{u}(k) \quad (4.9)$$

$$\mathbf{Q_1} = \mathbf{Q_1}^T \geq 0\ ,\ \mathbf{Q_2} = \mathbf{Q_2}^T > 0\ ,\ \begin{bmatrix} \mathbf{Q_1} & \mathbf{Q_{12}} \\ \mathbf{Q_{12}} & \mathbf{Q_2} \end{bmatrix} \geq 0$$

for the discrete case, where $\mathbf{Q_1}$, $\mathbf{Q_2}$, and $\mathbf{Q_{12}}$ are constant matrices used for tuning, and k and N are the discrete time index and the horizon to minimize over, respectively. The variable $\mathbf{x}(k)$ is the state vector of the system and $\mathbf{u}(k)$ is the control signal on the form

$$\mathbf{u}(k) = -\mathbf{L}\,\mathbf{x}(k)\ . \quad (4.10)$$

The optimal control law $\mathbf{L}$ (for the undisturbed case) is found by solving the discrete algebraic Riccati equation

$$\mathbf{S} = \mathbf{A}^T\mathbf{S}\mathbf{A} + \mathbf{Q_1} - \left(\mathbf{A}^T\mathbf{S}\mathbf{B} + \mathbf{Q_{12}}\right)\left(\mathbf{Q_2} + \mathbf{B}^T\mathbf{S}\mathbf{B}\right)^{-1}\left(\mathbf{B}^T\mathbf{S}\mathbf{A} + \mathbf{Q_{12}}^T\right)\ ,$$

and using the controller with

$$\mathbf{L} \;=\; \left(\mathbf{Q_2} + \mathbf{B}^T\mathbf{S}\mathbf{B}\right)^{-1}\left(\mathbf{B}^T\mathbf{S}\mathbf{A} + \mathbf{Q_{12}}^T\right)\ .$$

Kalman Predictor and Filter

If the states are not measured, they can be estimated. The description of estimators presented here follows that of Åström and Wittenmark (1997). The design of estimators is based on the state–space model

$$\begin{aligned} \mathbf{x}(k+1) &= \mathbf{A}\,\mathbf{x}(k) + \mathbf{B}\,\mathbf{u}(k) + v(k) \\ \mathbf{y}(k) &= \mathbf{C}\,\mathbf{x}(k) + z(k) \end{aligned}\ ,$$

with zero mean noise processes $\{v(k)\}$ and $\{z(k)\}$ and covariance

$$\mathrm{E}\left\{ \begin{bmatrix} v(k) \\ z(k) \end{bmatrix} \begin{bmatrix} v(k) \\ z(k) \end{bmatrix}^T \right\} = \begin{bmatrix} \mathbf{R_1} & \mathbf{R_{12}} \\ \mathbf{R_{12}}^T & \mathbf{R_2} \end{bmatrix} \quad ,$$

A predictive estimator can be formulated as

$$\hat{\mathbf{x}}(k+1) \quad = \quad (\mathbf{A} - \mathbf{KC})\, \hat{\mathbf{x}}(k) + \mathbf{B}\,\mathbf{u}(k) + \mathbf{K}_m\,\mathbf{y}(k), \qquad (4.11)$$

The Kalman predictor used is given by the choice of the stationary Kalman gain $\mathbf{K}_m$ that minimizes the variance of the estimation error $\tilde{\mathbf{x}} = \mathbf{x} - \hat{\mathbf{x}}$

$$\mathrm{E}\left\{ \left(\tilde{\mathbf{x}}(k+1) - \mathrm{E}\left\{\tilde{\mathbf{x}}(k+1)\right\}\right) \left(\tilde{\mathbf{x}}(k+1) - \mathrm{E}\left\{\tilde{\mathbf{x}}(k+1)\right\}\right)^T \right\}.$$

This expression is minimized by solving the discrete algebraic Riccati equation

$$\mathbf{P} = \mathbf{APA}^T + \mathbf{R_1} - \left(\mathbf{APC}^T + \mathbf{R_{12}}\right) \left(\mathbf{CPC}^T + \mathbf{R_2}\right)^{-1} \left(\mathbf{CPA}^T + \mathbf{R_{12}}^T\right)$$

with

$$\mathbf{K}_m \quad = \quad \left(\mathbf{APC}^T + \mathbf{R_{12}}\right) \left(\mathbf{R_2} + \mathbf{CPC}\right)^{-1} \quad .$$

The predictive estimator of Eq. (4.11) estimates the state without direct term—that is, a measurement taken at time $k-1$ does not propagate to the estimate until time k, causing one sample–time delay. If the measurement at time k is available for estimation, a second update step can be added to the estimation;

$$\begin{aligned} \hat{\mathbf{x}}(k \mid k-1) \quad &= \quad (\mathbf{A} - \mathbf{K}_m\mathbf{C})\, \hat{\mathbf{x}}(k \mid k-1) + \mathbf{B}\,\mathbf{u}(k-1) + \mathbf{K}_m\,\mathbf{y}(k-1). \\ \hat{\mathbf{x}}(k \mid k) \quad &= \quad \hat{\mathbf{x}}(k \mid k-1) + \mathbf{K}_f\left(\mathbf{y}(k) - \mathbf{C}\hat{\mathbf{x}}(k \mid k-1)\right) \quad , \end{aligned}$$

which is the Kalman filter for the optimal choice of $\mathbf{K}_f$. The notation $\hat{\mathbf{x}}(k \mid k-1)$ indicates the state estimate at time k based on measurements up until, and including time $k-1$. The variance of $\hat{\mathbf{x}}(k \mid k)$ is minimized by the choice

$$\mathbf{K}_f \quad = \quad \mathbf{PC}^T \left(\mathbf{CPC}^T + \mathbf{R_2}\right)^{-1} \quad .$$

It should be noted that $\mathbf{P}$ here denotes the variance of the predicted estimate $\mathbf{P}(k \mid k-1)$. The variance of the filtered estimate $\mathbf{P}(k \mid k)$ is smaller or equal to $\mathbf{P}(k \mid k-1)$.

4.4 LQR Control and the Kalman Predictor/Filter

If only the measurement of time $k-1$ is available for the calculation of the control signal at time k , the control law of Eq. (4.10) must be based on the predictive estimator of Eq. (4.11), so that

$$\mathbf{u}(k) = -\mathbf{L}\,\hat{\mathbf{x}}(k) \ ,$$

where $\hat{\mathbf{x}}(k)$ is obtained from Eq. (4.11).

If the measurement of time k is available for the calculation of the control signal at time k, the estimation of $\hat{\mathbf{x}}(k \mid k)$ can be included in the control law, and by rearranging, formulated as a predictor based feedback law with direct term

$$\begin{aligned}
\mathbf{u}(k) &= -\left(\mathbf{L} - \mathbf{L}\mathbf{K}_f\mathbf{C} - \mathbf{L}_\mathbf{v}\mathbf{K}_v\mathbf{C}\right)\hat{\mathbf{x}}(k \mid k-1) - \left(\mathbf{L}\mathbf{K}_f + \mathbf{L}_\mathbf{v}\mathbf{K}_v\right)\mathbf{y}(k) \\
\mathbf{L}_\mathbf{v} &= \left(\mathbf{Q_2} + \mathbf{B}^T\mathbf{S}\mathbf{B}\right)^{-1}\mathbf{B}\mathbf{S} \\
\mathbf{K}_v &= \mathbf{R_{12}}\left(\mathbf{C}\mathbf{P} + \mathbf{R_2}\right)^{-1} \ ,
\end{aligned}$$

where $\hat{\mathbf{x}}(k \mid k-1)$ is estimated by the Kalman predictor in Eq. (4.11) [Åström and Wittenmark, 1997]. This solution does not suffer from the time delay of the Kalman predictor implementation. Furthermore, the state estimation of time k can be calculated before the measurement of time k is taken, resulting in a small computational delay between the measurement and control signal update.

5

Identification and Validation Results

5.1 Experiments

Experiment # 1 – Servo Valve Validation

To identify the servo valve dynamics, two sequences were applied to the position estimate reference; a PRBS sequence for model estimation and a step sequence for visual validation. The PRBS sequence contained mainly energy in the frequency range 0-1000 Hz.

Experiment # 2 – Model Identification of FAC

For this experiment both the primary and the secondary combustion chamber were included. Two equivalent experiments of 1.6 s (16,000 samples) each were performed, denoted the identification data set and the validation data set. The input to the valve reference for both experiments was a PRBS signal, exciting the dynamics in the frequency domain 0-1000 Hz. The fuel supply was approximately 0.75 l/min for both sequences.

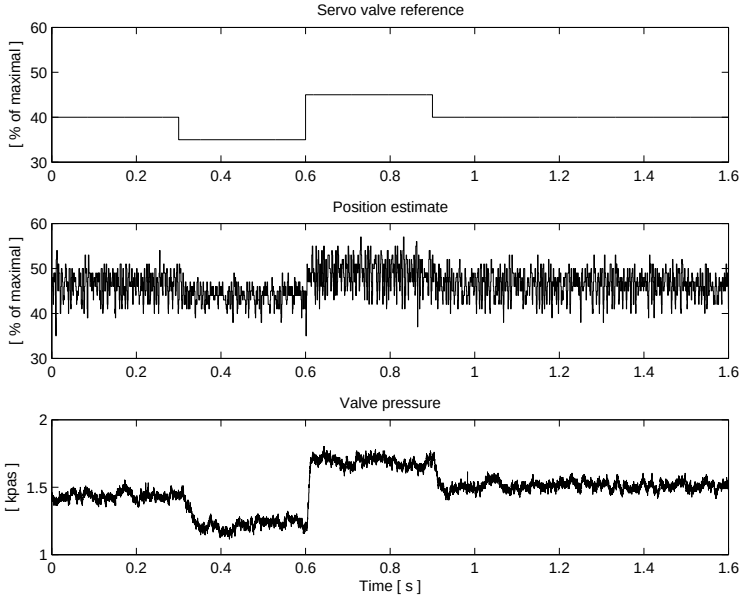

Figure 5.1 Servo valve response to reference changes. Top: Position estimate reference. Middle: Position estimate. Bottom: Valve pressure response. It is assumed that the mass flow is a static monotone function of the valve pressure.

5.2 Fast Fuel–Actuator

The servo valve validation tests were all based on data from experiment #1. Figure 5.1 illustrates the position estimate and the valve pressure response to a sequence of steps in the position estimate reference.

To estimate the dynamic properties of the servo valve, the relationship between the position estimate reference and the valve pressure was estimated both by the CVA and by the MOESP method. The Bode–diagram of the two models are illustrated in Fig. 5.3. The model order and sample frequency were chosen $n = 5$ and 1.25 kHz, respectively. The prediction accuracy of the models are illustrated in Fig. 5.2 for visual model validation.

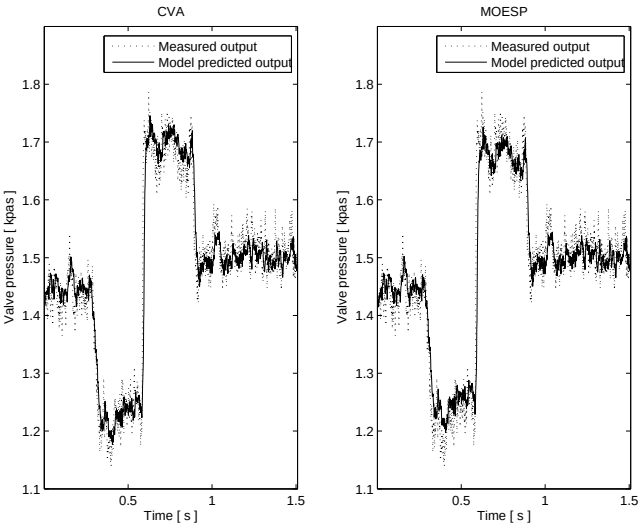

Figure 5.2 Prediction accuracy of model estimated with CVA and MOESP. The dotted lines illustrate the measured valve pressure response in the test sequence, and the full lines represent the 10–step ahead (4 ms) predicted model output.

Table 5.1 summarizes the model identification results.

Table 5.1 Summary of model identification of servo valve.

Identification method	Model order	κ_f* [%]	κ_v* [%]
CVA	5	72.4	92.4
MOESP	5	71.1	91.6

* 10–step ahead prediction was imposed in all cases.

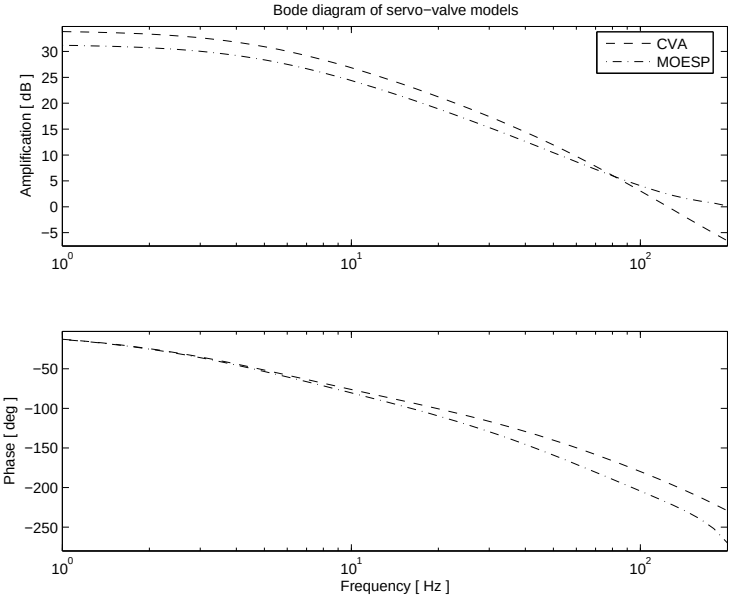

Figure 5.3 Bode diagram of the identified servo–valve models (via the CVA and MOESP method).

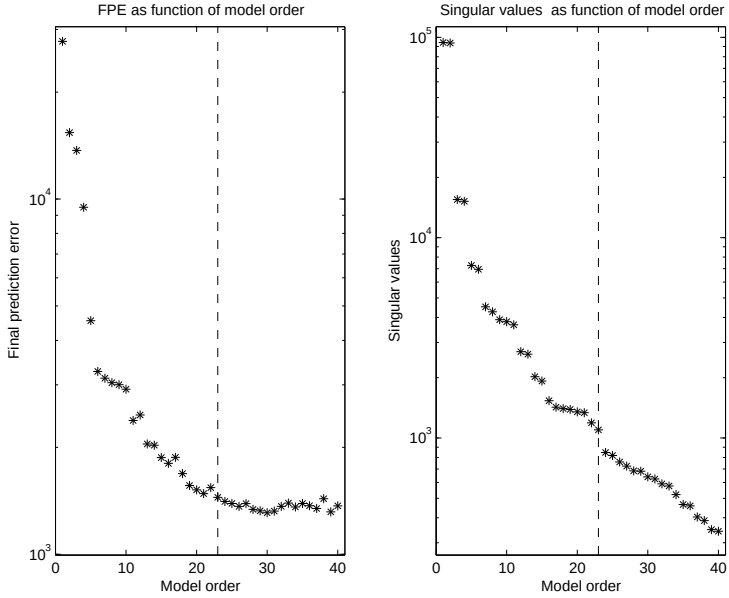

Figure 5.4 Left: FPE of the identified model using the CVA method as function of the model order. Right: Singular values as function of the model order. The dashed lines indicate the model order $n = 23$.

5.3 Identification of FAC Dynamics

This section describes the identification of models of the fuel actuated combustion chamber. All models are single–input single–output with the servo valve reference as input and the upstream combustion chamber pressure as output, unless stated differently.

Model Order Determination

Figure 5.4 illustrates the final prediction error and the singular values based on the measurements from experiment #2. A model order of $n = 23$ was appropriate both according to the FPE and the singular values.

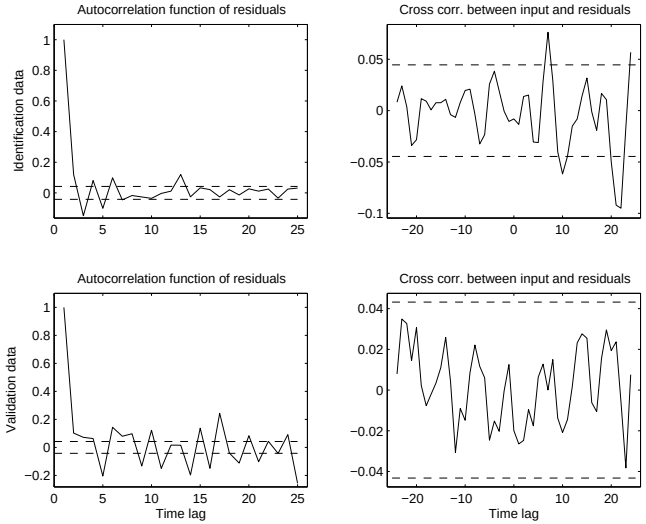

Figure 5.5 Residual test for MOESP identifications (model #2). Upper row: Residual tests based on identification data. Lower row: Residual tests based on validation data. Left column: Autocorrelation function of residuals. Right column: Cross correlation between input and residuals. The dashed lines indicate the 99% confidence intervals.

Model 2—Identification by the MOESP Method

The identification of the FAC was based on the two data sets from experiment #2 where the input was the servo valve reference and the output was the upstream pressure sensor. The model was identified using the MOESP method with a model order of $n = 23$. The top of Fig. 5.5 illustrates how the residuals of the identification data were autocorrelated and cross correlated with the input, respectively. Both figures indicate insignificant correlation, which again indicates that all statistical information of dynamics has been extracted from the data. For validation the bottom of Fig. 5.5 illustrates how the residuals of the validation data were autocorrelated and cross correlated with the input, respectively. The results here indicate a little more correlation than for the identification data, but not significantly more.

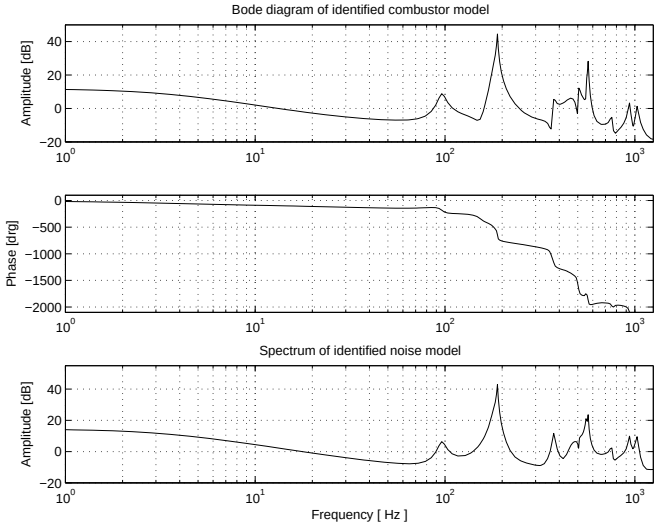

Figure 5.6 Bode diagrams for the model estimated with MOESP (model #2). Top and middle: Amplitude and phase diagram for the relationship between valve reference and combustion chamber pressure perturbations. Bottom: Amplitude diagram for the relationship between noise and combustion chamber pressure perturbations.

Figure 5.7 illustrates the prediction accuracy of the model. Here a 4 ms–step ahead prediction was imposed, and it shows well predicted model outputs. The prediction fit and variance-accounted-for for this test were $\kappa_f = 61.1\%$ and $\kappa_v = 84.9\%$.

The top and middle of Fig. 5.6 illustrate the Bode diagram of the identified model. It captures the dominating resonance frequency well, and a less dominating resonance frequency is observed at a lower frequency. The phase plot indicates a significant time delay in the system. The bottom of Fig. 5.6 illustrates the gain of the Bode diagram from the noise to the output.

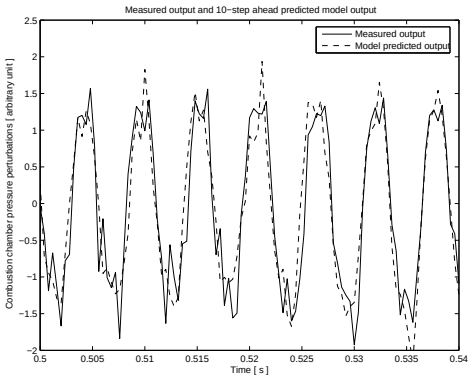

Figure 5.7 Prediction accuracy of the model estimated with MOESP (model #2). Measured output (full line) and 10–step ahead (4 ms) predicted model output based on identification data (dashed line).

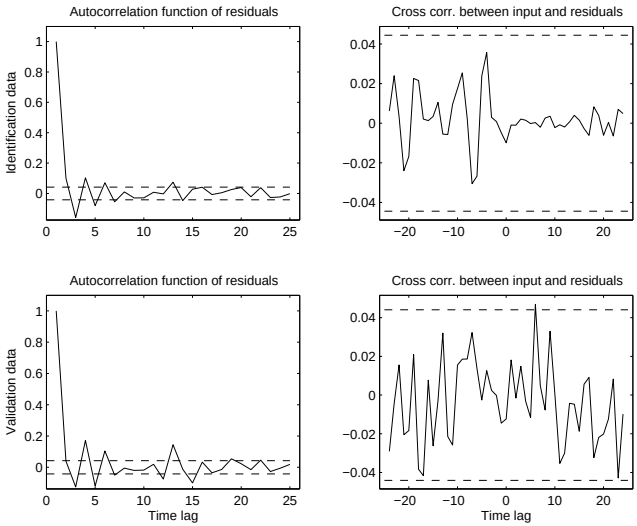

Figure 5.8 Residual test for CVA (model #3). Upper row: Residual tests based on identification data. Lower row: Residual tests based on validation data. Left column: Autocorrelation function of residuals. Right column: Cross correlation between input and residuals. The dashed lines indicate the 99% confidence intervals.

Model 3—Identification by the CVA Method

The identification of the FAC dynamics was based on the two data sets from experiment #2, where the input was the servo valve reference and the output was the upstream pressure sensor. The model was identified using the CVA method with a model order of $n = 23$. The top of Fig. 5.8 illustrates how the residuals of the identification data were autocorrelated and cross correlated with the input, respectively. Both figures indicate only insignificant correlation, which again indicates that all statistical information of dynamics has been extracted from the data. For validation, the bottom of Fig. 5.8 illustrates how the residuals of the validation data were autocorrelated and cross correlated with the input, respectively. These results indicate a bit more correlation than the identification data, but not significantly more. Figure 5.10 illus-

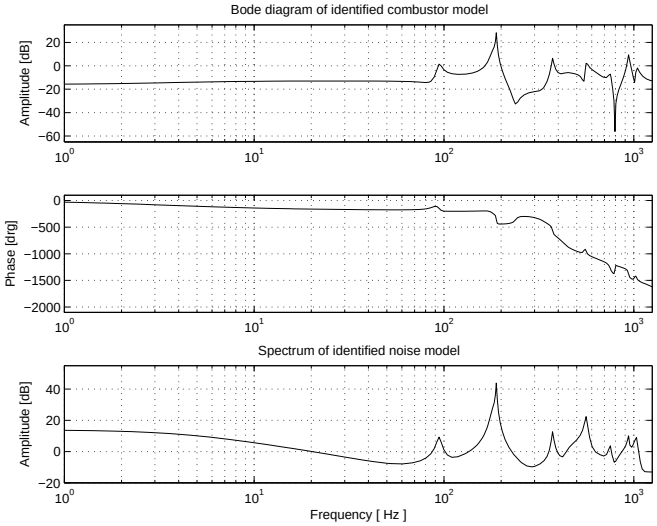

Figure 5.9 Bode diagrams for identified model estimated with CVA (model #3). Top and middle: Amplitude and phase diagram for the relationship between valve reference and combustion chamber pressure perturbations. Bottom: Amplitude diagram for the relationship between noise and combustion chamber pressure perturbations.

trates the prediction accuracy of the model. Here a 4 ms–ahead prediction was imposed, and it shows well predicted model outputs. The prediction fit and variance-accounted-for for this test were $\kappa_f = 80.1\%$ and $\kappa_v = 96.0\%$.

The top and middle of Fig. 5.9 illustrate the Bode diagram of the identified model. It captures the dominating resonance frequency well, and a less dominating resonance frequency is observed at a lower frequency. The phase plot indicates a significant time delay in the system. The bottom of Fig. 5.9 illustrates the gain of the Bode diagram from the noise to the output.

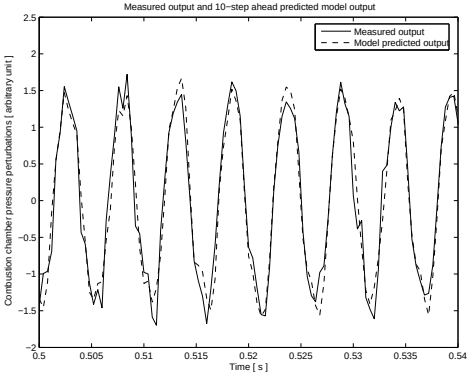

Figure 5.10 Prediction accuracy of model estimated with CVA (model #3). Measured output (full line) and 10–step ahead (4 ms) predicted model output based on identification data (dashed line).

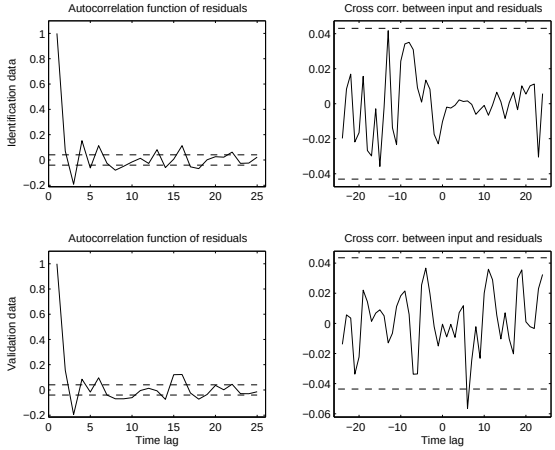

Figure 5.11 Residual test for CVA (model #4). Upper row: residual tests based on identification data. Lower row: Residual tests based on validation data. Left column: Autocorrelation function of residuals. Right column: Cross correlation between input and residuals. The dashed lines indicate the 99% confidence intervals.

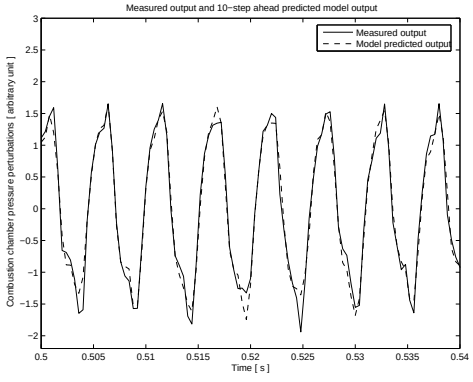

Figure 5.12 Prediction accuracy of model estimated with CVA (model #4). Measured output (full line) and 10–step ahead (4 ms) predicted model output based on identification data (dashed line).

Model 4—Identification by the CVA Method II

The identification of the FAC dynamics was based on the two data sets from experiment #2. The model was identified using the CVA method with a model order of $n = 16$. The top of Fig. 5.11 illustrates how the residuals of the identification data were autocorrelated and cross correlated with the input, respectively. Both figures indicate only insignificant correlation, which again indicates that all statistical information of dynamics has been extracted from the data. For validation the bottom of Fig. 5.11 illustrates how the residuals of the validation data were autocorrelated and cross correlated with the input, respectively. Figure 5.12 illustrates the prediction accuracy of the model. Here a 4 ms–ahead prediction was imposed, and it shows well–predicted model outputs. The prediction fit and variance-accounted-for for this test were $\kappa_f = 79,5\%$ and $\kappa_v = 95,8\%$.

The top and middle of Fig. 5.13 illustrate the Bode diagram of the identified model. It captures the dominating resonance frequency well. The phase plot indicates a significant time delay in the system. The bottom of Fig. 5.13 illustrates the gain of the Bode diagram from the noise to the output.

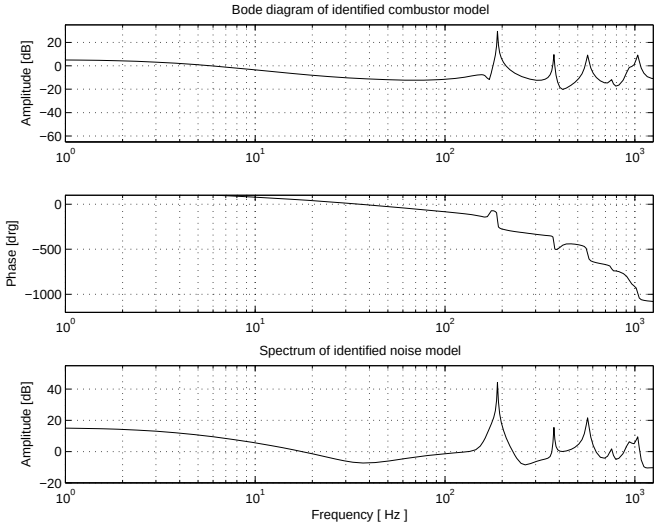

Figure 5.13 Bode diagrams for identified model estimated with CVA (model #4). Top and middle: Amplitude and phase diagram for the relationship between the valve reference and combustion chamber pressure perturbations. Bottom: Amplitude diagram for the relationship between noise and combustion chamber pressure perturbations.

Model 5—Identification by the CVA Method (SIMO)

A single–input multiple–output (SIMO) model of the FAC was estimated based on the two data sets from experiment #2. The outputs were the servo valve position estimate, the valve pressure, and the upstream combustion chamber pressure. The model was identified using the CVA method with a model order of $n = 22$. Validation results of the identification are illustrated in Fig. 5.14. The prediction fit and variance-accounted-for for the prediction of i_{pos}, p_v, and p_u were (ordered) $\kappa_f = (2.7, 38.7, 79.4)\%$ and $\kappa_v = (5.3, 62.4, 95.8)\%$.

Figure 5.15 illustrate the gain diagrams of the identified model.

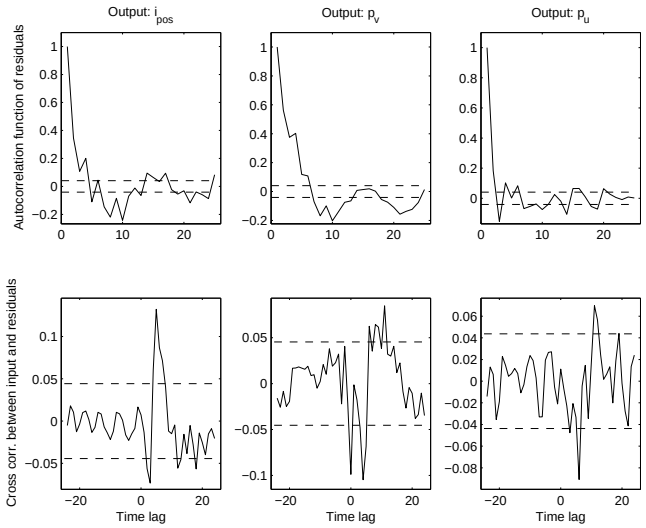

Figure 5.14 Residual test for CVA (model #5). Top row: Autocorrelation function of residuals for validation date. Bottom row: Cross correlation between input and residuals for validation data. First column to last column: Servo valve position estimate, valve pressure, and combustion chamber pressure at the upstream pressure sensor. The dashed lines indicate the 99% confidence intervals.

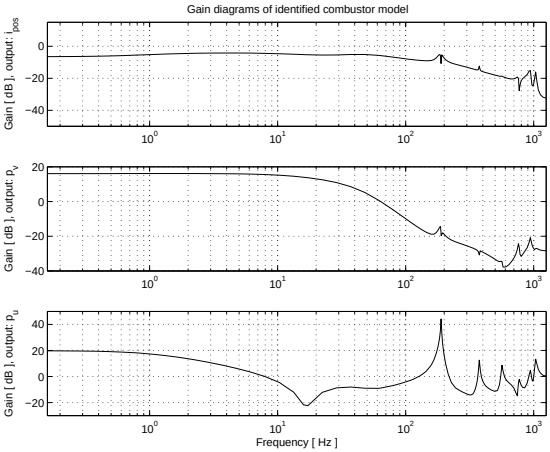

Figure 5.15 Gain diagrams for identified SIMO model estimated with CVA (model #5). The input is the servo valve reference and the outputs are from top to bottom; the servo valve position estimate, the valve pressure, and the combustion chamber at the upstream pressure sensor.

5.4 Summary of Model Identification Results

Table 5.2 summarizes the model identification results.

Table 5.2 Summary of model identification.

Model no.	Identification method	Order	κ_f* [%]	κ_v* [%]
#2	MOESP	23	61.1	84,9
#3	CVA	23	81,1	96.6
#4	CVA	16	79.5	95.8
#5	CVA	24	2.7,38.7,79.4	5.3,62.4,95.8

* 10–step ahead prediction was imposed in all cases.

6

Control Design and Results

The control designs investigated are presented in this chapter. The control designs for the PAC and the FAC are first presented, and a section describes some practical details concerning the performed experiments. Finally, at the end of the chapter, the experimental results are presented.

6.1 Control Design for PAC

Control 1—Proportional Control

Since the bandwidth of the loudspeaker was much higher than the pressure oscillations, the root locus of the system described by Eq. (4.8) was as illustrated in Fig. 6.1, which illustrates the qualitative behavior of the poles of the closed–loop system, if proportional control was imposed. It shows that for any control gain, the closed–loop system remained stable (all poles remained within the left hand side of the pole–zero diagram). As long as the model described the real system, the combustion chamber pressure could be stabilized by proportional control with any gain. However, due to model uncertainty the choice of control gain was critical to the pressure stabilization in practice. The gain was tuned by hand until damping of the oscillations was obtained.

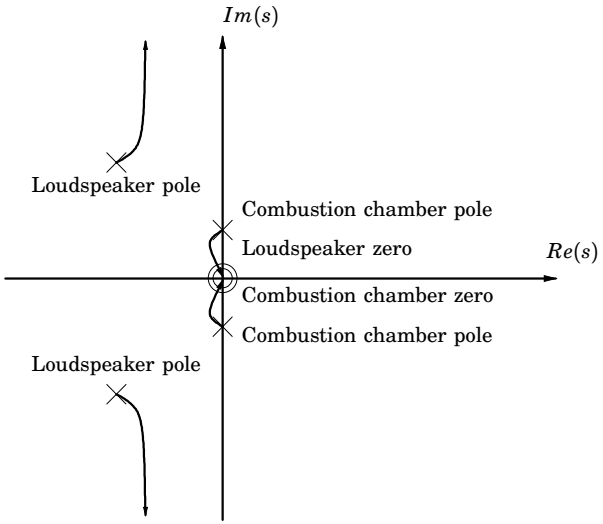

Figure 6.1 Root locus of pressure actuated combustion chamber. The input and output are the voltage over the loudspeaker and the pressure at the downstream pressure sensor, respectively. Note that this is only a qualitative illustration, and it contains no information about the exact locations of the poles and zeros.

6.2 Control Design for FAC

Control 2—Loop–Shaping Control

The loop–shape controller was designed to shape the Bode diagram of model #2 (identified by the MOESP method). The servo valve had a drop in magnitude at low frequency, which was compensated by a lead network. Two notch filters were included to reduce the effect of the lowest resonance frequencies; one at the dominating resonance frequency, and one damping a lower frequency resonance frequency. Finally, a fifth order low–pass filter was inserted to suppress the effect of higher frequency resonances.

The Bode diagram of the loop–shape controller is illustrated in Fig. 6.2. Figure 6.3 illustrates the Nyquist diagram of the loop–shape con-

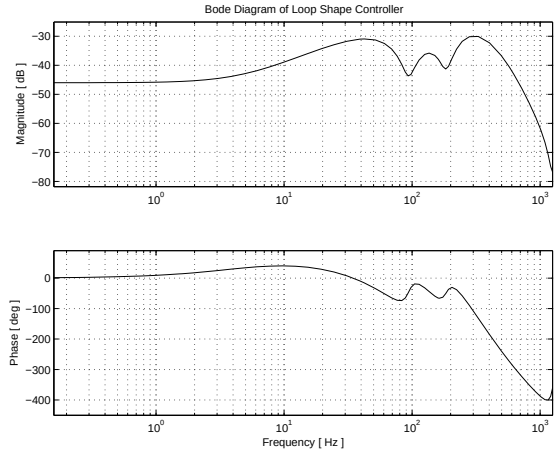

Figure 6.2 Bode plot of loop–shape controller.

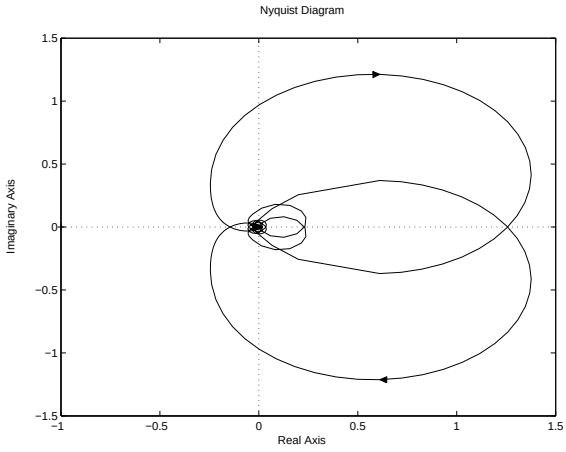

Figure 6.3 Nyquist diagram of the loop–transfer function of the combined loop–shape controller and model #2 identified with the MOESP method.

troller and model #2 identified with the MOESP method.

Control 3—LQR Control with Penalized Derivative

This control design was based on the LQR method and model #3 (identified by the CVA method).

Since the estimated model for this setup only described the relationship between the servo valve reference and the combustion chamber pressure at the upstream pressure sensor, it was chosen to base the control design on these variables. The cost function to be minimized was

$$J = \sum_{k=0}^{\infty} \left[p_u(k)^2 + \alpha \left(p_u(k+1) - p_u(k) \right)^2 + \beta u_{sv}(k)^2 \right] \tag{6.1}$$

where the variable $p_u(k)$ was the measured pressure perturbation at the upstream pressure sensor. The first term penalized the actuation signal in order to respect the operating range of the servo valve. The second term penalized the pressure perturbation in order to suppress the pressure oscillations. To put further focus on the oscillation suppression, the pressure difference between two following samplings were also penalized by the third term in Eq. (6.1). The weighting of the penalization could be adjusted by the two tuning parameters α and β. Equation (6.1) could be transformed into the state–space formulation described in Eq. (4.9) by defining the matrices

$$\begin{aligned} \mathbf{Q_1} &= \mathbf{C}^T \mathbf{C} + \alpha \left(\mathbf{C}\mathbf{A} - \mathbf{C} \right)^T \left(\mathbf{C}\mathbf{A} - \mathbf{C} \right) \\ \mathbf{Q_2} &= \alpha \mathbf{B}^T \mathbf{C}^T \mathbf{C} \mathbf{B} + \beta \\ \mathbf{Q_{12}} &= \alpha \left(\mathbf{C}\mathbf{A} - \mathbf{C} \right)^T \mathbf{C}\mathbf{B}. \end{aligned} \tag{6.2}$$

The minimization problem was solved by tools in the Matlab® Control System Toolbox®.

The implemented control consisted of the Kalman predictor and the control law obtained as described above, which were combined to

$$\begin{aligned} \hat{\mathbf{x}}(k+1) &= \left(\mathbf{A} - \mathbf{K}\mathbf{C} - \mathbf{B}\mathbf{L} \right) \hat{\mathbf{x}}(k) + \mathbf{K} p_u(k) \\ u_{sv}(k) &= -\mathbf{L}\hat{\mathbf{x}}(k) \end{aligned} \tag{6.3}$$

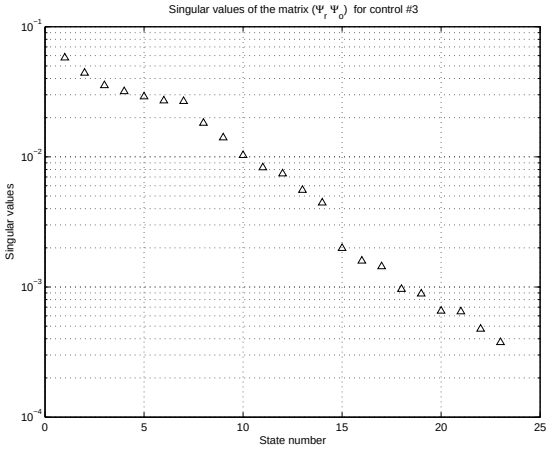

Figure 6.4 Singular values of the matrix ($\mathbf{\Psi}_r\mathbf{\Psi}_o$) for the estimator based LQR controller.

where the variable $\hat{\mathbf{x}}$ was the estimated state vector. Because the control design was based on a model with sampling frequency of 2.5 kHz, the control was implemented with this sampling frequency as well. For implementation issues the controller was reduced, using the balanced model reduction method. Figure 6.4 illustrates the singular values of the matrix ($\mathbf{\Psi}_r\mathbf{\Psi}_o$), associated with the balanced realization of the estimator based LQR controller (Eq. (6.3)). A model order of $n = 15$ resulted only in small deviation of the reduced model Bode diagram compared to the full order controller. Figure 6.5 illustrates the Nyquist diagram of the loop transfer function of the designed LQR controller and the identified model. It is noted that the amplification could be increased without losing stability, but was avoided because of actuator limitations.

Control 4—LQR Control with Penalized Derivative and Direct Term

This control design was based on the LQR method and model #4 (identified by the CVA method). The design was based on the same cost

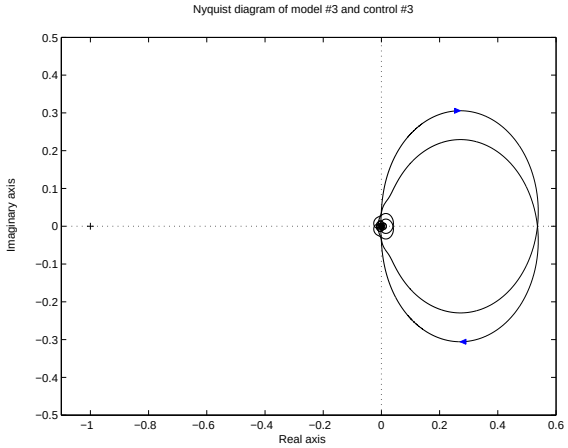

Figure 6.5 Nyquist diagram of the loop transfer–function of the combined LQR controller (with Kalman predictor) and model #3 the identified the with CVA method.

function as the design of control #3, see Eq. (4.9) and (6.2). The state estimate was obtained by a Kalman filter with anti wind–up, implemented as

$$\begin{aligned}\hat{\mathbf{x}}(k+1) &= (\mathbf{A} - \mathbf{K}_x\mathbf{C})\,\hat{\mathbf{x}}(k) + \mathbf{B}\,u_{sv}(k) + \mathbf{K}_x\,p_u(k)\\ u_t(k) &= -(\mathbf{L} - \mathbf{L}\mathbf{K}_f\mathbf{C} - \mathbf{L}_\mathbf{v}\mathbf{K}_v\mathbf{C})\,\hat{\mathbf{x}}(k) - (\mathbf{L}\mathbf{K}_f + \mathbf{L}_\mathbf{v}\mathbf{K}_v)\,p_u(k)\\ u_{sv}(k) &= sat(u_t(k))\end{aligned}$$

where $sat(\cdot)$ was a suitable saturation function describing the limitations in the actuator.

Figure 6.6 illustrates the Nyquist diagram of the loop transfer–function of model #4 and the LQR controller with Kalman filter. It is noted that the amplification could be increased without loosing stability, but this approach was not further considered due to actuator limitations.

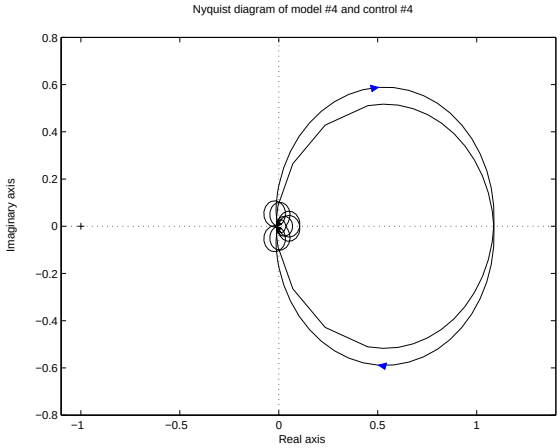

Figure 6.6 Nyquist diagram of the loop transfer function of the combined LQR controller (with Kalman filter) and model #4 identified with the CVA method.

6.3 Control Experiments

For all experiments two data sequences were recorded; the first without active control, the second with. Both experiments were performed with the same averaged valve pressure (to ensure the same fuel flow). In all cases, the fuel supply was approximately 0.75 l/min. Table 6.1 lists further details on the individual experiments.

6.4 Data Processing

Variance Ratio

The variance ratio η_v is defined to compare the combustion chamber pressure perturbation of the actively controlled experiment with that of the uncontrolled. The variance ratio is defined by

$$\eta_v = \frac{\mathrm{var}\left(\{p_d\}_N^c\right)}{\mathrm{var}\left(\{p_d\}_N^{uc}\right)}$$

where N is the number of samples in each data sequence, and $\{p_d\}_N^c$ and $\{p_d\}_N^{uc}$ are the sequences of active controlled and uncontrolled combustion pressure perturbations, respectively.

Spectrum Analysis

All spectral representation of experimental data are treated according to App. A.1, with smoothening window length of 4% of the sample size. These data are normalized so that the variance of the uncontrolled sequence is one.

Table 6.1 Summary of experiment conditions.

Exp. no.	Actuator	Pressure sensor	Time duration of sequences	Secondary combustion chamber included	Control
#3	P	D	31 s	no	#1
#4	P	D	31 s	no	#1
#5	FF	U	31 s	yes	#2
#6	FF	U	20 s	yes	#2
#7	FF	U	31 s	yes	#3
#8	FF	U	31 s	yes	#3
#9	FF	U	31 s	yes	#4
#10	FF	U	31 s	yes	#4

P: Pressure actuated. FF: Fast fuel actuated.
U: Upstream. D: Downstream

6.5 Control Results

Control of PAC with Control #1: Figures 6.7 and 6.8 illustrate the pressure actuated control results from experiments #3 and #4.

Control of FAC with Control #2: Figures 6.9 and 6.10 illustrate the pressure actuated control results from experiments #5 and #6.

Control of FAC with Control #3: Figures 6.11 and 6.12 illustrate the pressure actuated control results from experiments #7 and #8.

Control of FAC with Control #4: Figures 6.13 and 6.14 illustrate the pressure actuated control results from experiments #9 and #10.

Table 6.2 on page 83 lists further details.

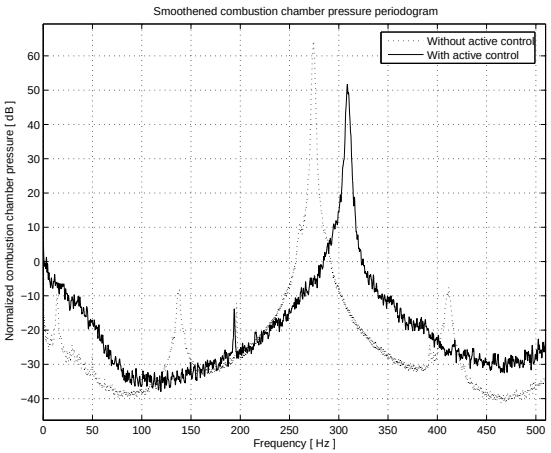

Figure 6.7 Smoothened combustion chamber pressure power spectrum of experiment #3: Pressure actuation with proportional control.

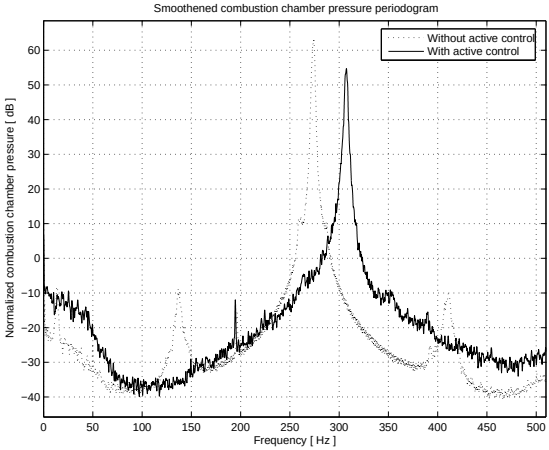

Figure 6.8 Smoothened combustion chamber pressure power spectrum of experiment #4: Pressure actuation with proportional control.

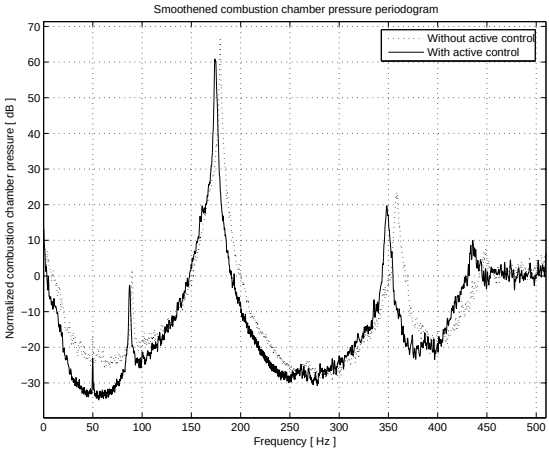

Figure 6.9 Smoothened combustion chamber pressure power spectrum of experiment #5: Fast–fuel actuation with loop–shaping control.

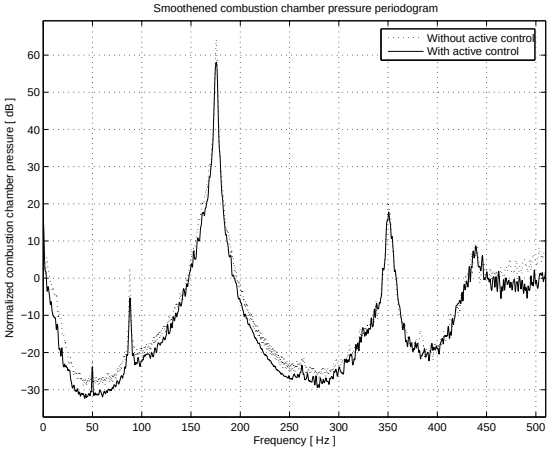

Figure 6.10 Smoothened combustion chamber pressure power spectrum of experiment #6: Fast–fuel actuation with loop–shaping control.

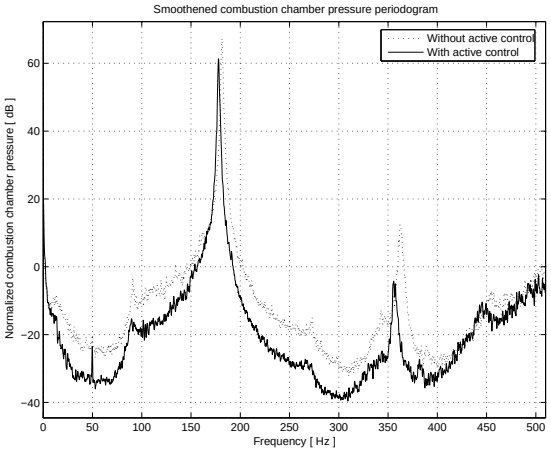

Figure 6.11 Smoothened combustion chamber pressure power spectrum of experiment #7: Fast–fuel actuation with LQR control with penalized derivative.

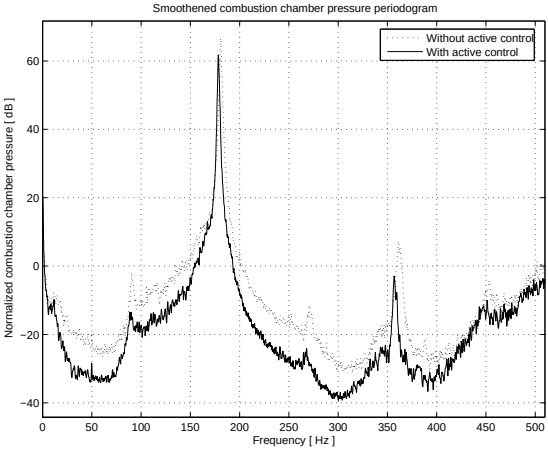

Figure 6.12 Smoothened combustion chamber pressure power spectrum of experiment #8: Fast–fuel actuation with LQR control with penalized derivative.

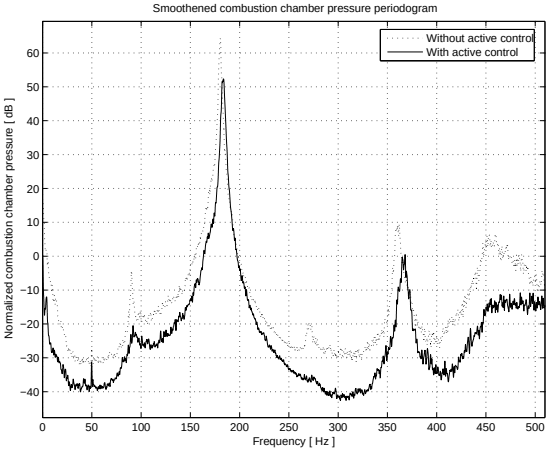

Figure 6.13 Smoothened combustion chamber pressure power spectrum of experiment #9: Fast–fuel actuation with LQR control with penalized derivative and direct term.

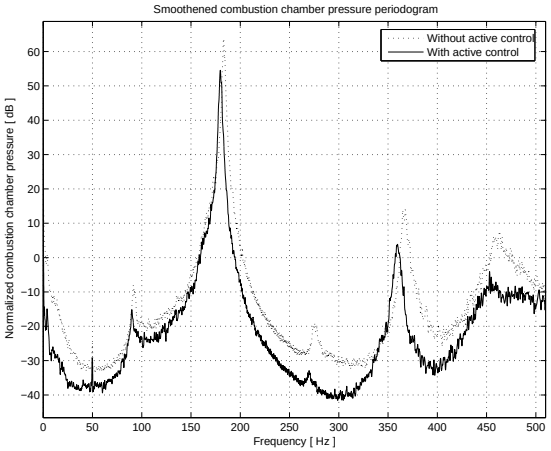

Figure 6.14 Smoothened combustion chamber pressure power spectrum of experiment #10: Fast–fuel actuation with LQR control with penalized derivative and direct term.

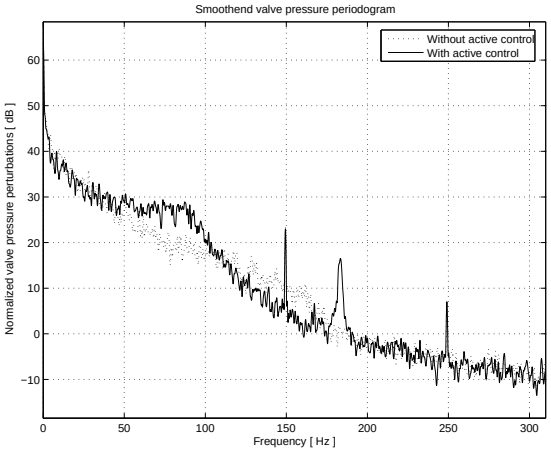

Figure 6.15 Smoothened valve pressure power spectrum of experiment #9.

6.6 Summary of Control Results

Table 6.2 summarizes the control results.

Table 6.2 Summary of control results.

Exp. no.	Actuator	Control	n	η_v	Damping of dominating resonance	Frequency shift of dominating resonance
#3	P	#1	0	0.32	13 dB	34 Hz
#4	P	#1	0	0.42	9 dB	33 Hz
#5	FF	#2	10	0.77	5 dB	-5 Hz
#6	FF	#2	10	0.71	6 dB	0.5 Hz
#7	FF	#3	15	0.50	6 dB	-3 Hz
#8	FF	#3	15	0.51	5 dB	-2 Hz
#9	FF	#4	16	0.37	12 dB	3 Hz
#10	FF	#4	16	0.38	9 dB	-3 Hz

P: Pressure actuated. FF: Fast fuel actuated.

7

Discussion

Several instabilities problems are related to the combustion process. In this thesis, the treatment of combustion instabilities is focused on the acoustic properties of the combustion process, and all conclusions and comments are based on this restriction.

7.1 Fast Fuel–Actuator

The design and implementation of the servo valve changed the binary behavior of the solenoid valve into proportional. Both the pressure and the position estimate changed according to the reference. Some small steady–state error could be observed in the experiments, since the valve pressure did not return to the initial value despite that the reference returned to the initial value (see Fig. 5.1). This steady state error could be removed by imposing integral effect in the position control loop, but since the valve was used for noise suppression, the steady state behavior was not of primary concern.

Since the solenoid valve was affected by a series of steps (due to the PFM signal), the position of the poppet inside the valve could not be expected to be steady, even for steady references. This is observed in the position estimate illustrated in Fig. 5.1. These oscillations are not seen in the valve pressure (the bottom of Fig. 5.1), indicating that the dynamic of the gas had some low–pass filter properties.

The time delay was estimated by assuming that the phase decay at frequencies above 16 Hz were due to the delay. First order polynomials

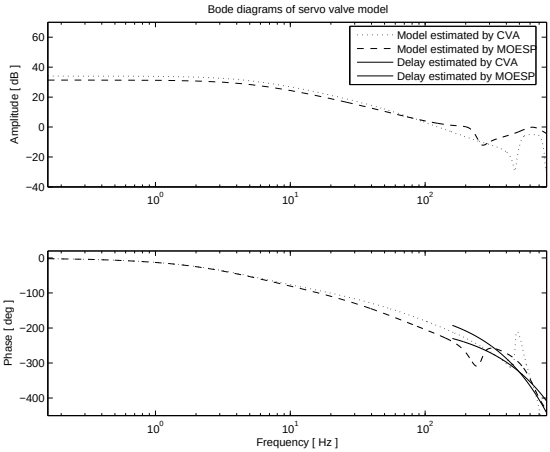

Figure 7.1 Bode diagrams of servo valve identified with the CVA and MOESPmethod. The full lines indicate the estimated time–delay phase contribution. The time delay is estimated to be in the order of 0.8-1.1 ms (by the MOESP and CVA method, respectively).

were fitted to the phase of the two models using least square fit. The polynomials are illustrated in Fig. 7.1 along with the Bode diagrams of the models. The estimated polynomials suggested a time delay of around 0.8-1.1 ms. This was in the order of one fifth of the period time of the dominating resonance frequency of the fuel actuated combustion chamber, approximately 2-3 sample steps for the fuel actuated combustion chamber models, and approximately one PFM cycle.

7.2 Modeling

Model formulations based on physical insight have the advantage of allowing intuitive understanding, which is a significant support for the design and tuning of a controller. The disadvantage of this method is that it can be time consuming, or in some cases even impossible. When such problems arise, system identification based on measurements is an alternative. When using such method, it is only required that the

process can be operated manually in a safe mode, and that the operator has some kind of actuating access and suitable measurement equipment. Based on data alone, there exist a number of numerical tools to estimate dynamic models.

Analytical Combustion Chamber Model

The analytical modeling of the pressure actuated combustion chamber model was possible because of the simple acoustic properties. The focus was to capture the acoustic properties, and the flame modeling was significantly neglected. The two assumptions

$$\begin{aligned} Q_f(s) &= \frac{b_1}{b_2} U_f(s) \\ 2\gamma p_0 &= \frac{b_1}{b_2} (\gamma - 1) \end{aligned}$$

were imposed. In particular the last was questionable, since any small deviation of any of the parameters would move the poles of the interconnected combustion model away from the imaginary axis. Excluding the assumptions above could result in an combustion model stable for some flame properties, and unstable for others. Such models were investigated [Rumsey *et al.*, 1998] and experimentally verified. These models explain the combustion instability as linear unstable growth until losses impose damping nonlinearities, leading to limit–cycle behavior.

The pressure actuated combustion chamber was investigated here only for proof of concept, not subject for excessive work. Therefore, it was chosen to derive as simple a model as possible in order to show the damping effect of active control. Based on this, it was chosen to compromise the physical interpretation of the model.

Subspace Identification of FAC

Two methods for system identification were tested; The MOESP and the CVA method. Both models captured the main resonance frequencies (compare Fig. 5.6, 5.9, and 5.13). However, the CVA method resulted in better prediction performance. The two estimation methods disagreed on the estimation of the low–frequency response, where the CVA method estimated significantly lower gains than the MOESP

method (compare Fig. 5.6 to Fig. 5.9). The two methods also disagreed on the estimation of the low–frequency amplification of the servo valve (see Fig. 5.3). Another disagreement was in the estimated phase. The MOESP method estimated earlier and steeper phase decrement. The noise estimations had reasonable agreement. It is concluded that the CVA method was preferable to the MOESP method in this specific application, due to its better prediction performance.

The choice of order had an interesting consequence; the higher order SISO models ($n = 23$) estimated a smaller resonance frequency around 94 Hz (see Fig. 5.6 and 5.9). The resonance was also observed in the measured output (see for example Fig. 6.9). The model identified by a lower order ($n = 16$) did not include this resonance frequency (see the Bode diagram in Fig. 5.13). Even though the control design based on the low–order model did not include information about this resonance, it suppressed it with 7 and 16 dB (see Fig. 6.13 and 6.14).

Only SISO models was utilized in the combustion control experiments presented. A SIMO model was derived to illustrate that the subspace–based method can be generalized to a more complex system (several outputs). This indicates that the method possibly can be utilized on more advanced combustion chambers. The prediction of the servo valve position estimate and the valve pressure showed not as high prediction indices as the prediction of the combustion chamber pressure. This indicates that further work (such as static compensation) might be needed before these measurements are included into the feedback.

7.3 Combustion Control with Pressure Actuation

The pressure actuator was relatively simple to implement in the simple combustion chamber presented in this thesis. It was mounted at a low–temperature zone, and it did not interact with the flow properties of the combustion chamber. In industrial combustion chambers, the implementation of loudspeakers causes severe problems due to the harsh conditions and high power requirements. However, in this thesis it was investigated for its illustrative benefits. The experiments indicated a significant noise reduction at the resonance frequencies, but poor noise suppression at others. This effect was expected to be due to the simple

controller. Further experiments with more complicated control design might provide better damping over a larger frequency range, but was not conducted, since the actuation method holds too severe complications for industrial applications [Dowling and Morgans, 2005]. Another interesting observation of the proportional pressure control experiments was the shift of the dominating resonance frequency; the experiments showed that the active–controlled resonance was approximately 34 Hz higher than the uncontrolled resonance. Whether or not this is regarded as an advantage is not to be determined here.

7.4 Combustion Control with Fast Fuel–Actuation

The results indicate that suppression of combustion oscillations is possible with fast fuel actuation. The experiments performed indicated that LQR holds the best potential of the tested design methods. Furthermore, it was the design method with least tuning complexity; only two weights had to be adjusted, whereas the loop–shape design method required much more insight and routine from the designer. It should be noted that the degrade in control performance of the loop-shape controller compared to the LQR controllers might also depend on the model used. The loop–shape controller was designed using the model identified by the MOESP method, which showed less attractive prediction properties than the models identified with the CVA method.

Of the two tested LQR implementations, the Kalman filter implementation showed superior to the Kalman predictor implementation. This comes as no surprise, since the Kalman filter incorporated the newest measurement in the current control signal. The importance of avoiding the time delay in the controller was enhanced by the lack of actuator bandwidth of the servo valve.

None of the fuel actuated control experiments resulted in any significant change in the dominating resonance frequency. This was not necessarily due to the actuator choice, but rather due to the control design. The design method imposed focused more on the overall noise suppression than on the resonance shift. The design of the proportional pressure controller only focused on the stabilization of the marginally stable poles, not on the final pole location, and the frequency shift might just be a side effect.

8

Conclusion and Future Work

This thesis addresses the problem of unstable combustion oscillations related to gas turbine applications. This type of instability is often observed in lean premixed combustors, which have potential for significant reduction of the emission levels, if stabilized. Active control is one solution to stabilize an unstable lean premixed combustion process.

8.1 Conclusions

To test different control strategies, a lean premixed combustion rig has been developed, allowing for pressure based feedback. A solenoid valve and a loudspeaker served as fuel and pressure actuators, respectively.

Modeling of Dynamics

The dynamics of the combustion chamber were modeled by using two different approaches; the pressure actuated combustion chamber was modeled analytically by governing equations, and the fuel actuated combustion chamber was modeled by using system identification. The system identification has the interesting property of not becoming extensively complicated to apply to more complex combustion chambers. Analytical models become extremely complex when industrial applications are considered, due to complicated geometry, more complex

chemistry, higher pressure, etc. The two system identification methods, applied in this work, holds no limitations to the SISO structure of the control strategies investigated. The methods can be applied to more complex combustors with more actuators and more sensors, without compromising the system identification methods.

Damping of Combustion Oscillations

The presented control algorithms are designed from different methods. For proof of concept, a pressure actuating proportional controller has shown capable of damping the main oscillation by 9-12 dB. This control strategy is theoretically advantageous, due to the high bandwidth of the actuator and the simple tuning. However, implementation issues exclude the loudspeaker from industrial applications. Furthermore, the proportional control strategy did not suppress the combustion oscillations over a wider frequency range.

The control designs applied to the fuel actuator showed different properties. The best results were obtained using LQR control. Experiments showed that including direct term and anti–windup in the controller, improved the damping of the combustion oscillations significantly. Results of 10-12 dB damping at the dominating frequency and a wide frequency range damping were obtained. This design is by far more relevant for industrial applications, since it requires no modification to existing combustion chambers.

The results indicates that fuel actuated feedback can be used to suppress combustion oscillations.

Fuel Actuator

One of the main limitations for the success of active combustion control is the actuator bandwidth. Many solutions have been proposed in the literature. This thesis presents a solution based on a solenoid valve with binary on–off characteristics, which is converted into graded behavior by applying inductive feedback. This servo valve design was shown to be capable of affecting combustion oscillations in the lean premixed combustion setup described in this thesis.

8.2 Future Work

Experiments have indicated what many others have reported [Dowling and Morgans, 2005], [Zinn, 2005]; the most critical limitation for active combustion control is the actuator bandwidth. Therefore more research in this field, with faster means of actuation is a natural continuation of the valve design presented in this thesis.

Industrial combustion chambers operate at pressures much higher than the atmospheric combustor described in this thesis. Operation under higher pressure is often avoided in laboratory experiments due to the much more complex structure. This difference in pressure conditions is often considered as the primary limiting factor between academic experiments and industrial applications. Applying the research, presented in this thesis, to a high pressure combustion chamber could serve to bridge this gap.

A deeper understanding of the physical phenomena of the combustion process, and the formulation of these as low–order dynamical models, could support the control design. Since many of the couplings in the combustion process are nonlinear, such models would naturally also have nonlinear elements. Because of the energy related dynamics, one obvious control design method could be the passivity approach (*passivity* is here related to the formalism of Khalil (2002), and is not related to the non–active control strategies described in Chapter 2).

The field of computational fluid dynamics is believed to hold much potential for active combustion control design. Using this type of analysis, control structures can be designed, modified, and tested in simulation environments. Here the environments of industrial combustion chambers can be simulated in a more safe and cheap manner, and the control configurations can be changed as needed.

9

Bibliography

Anderson, J. D. (1995): *Computational Fluid Dynamics, The Basics with Applications*. McGraw-Hill, Inc., Padston, UK.

Annaswamy, A. M., M. Fleifil, J. P. Hathout, and A. F. Ghoniem (1997): "Impact of linear coupling of the design of active controllers for the thermoacoustic instability." *Combustion Science and Technology*, **128**, pp. 131–180.

Annaswamy, A. M., M. Fleifil, J. W. Rumsey, R. Prasanth, J. P. Hathout, and A. F. Ghoniem (2000): "Thermoacoustic instability: Model-based optimal control designs and experimental validation." *Control Systems Technology*, **8:6**, pp. 905–918.

Annaswamy, A. M. and A. F. Ghoniem (2002): "Active control of combustion instability, theory and practice." *IEEE Control Systems Magazine*, December, pp. 37–54.

Åström, K. J. and T. Hägglund (2005): *Advanced PID Control*. ISA - The Instrumentation, Systems, and Automation Society, Research Triangle Park, NC.

Åström, K. J. and B. Wittenmark (1997): *Computer-Controlled Systems*. Prentice Hall, Upper Saddle River, NJ.

Bahr, D. W. (1999): "Gas turbine combustion and emission abatement technology current and projected status." In *Proceedings of the International Gas Turbine Congress*, vol. 1, pp. 15–25. Kobe, Japan.

Barooah, P., T. J. Anderson, and J. M. Cohen (2003): "Active combustion instability control with spinning valve actuator." *Journal of Engineering for Gas Turbines and Power*, **125**, pp. 925–932.

Cheung, N. C., K. W. Lim, and M. F. Rahman (1993): "Modelling a linear and limited travel solenoid." In *Proceedings of the International Conference on Industrial Electronics, Control, and Instrumentation, proceedings of the IECON '93.*, vol. 3, pp. 1567–1572. Maui, Hawaii.

Christensen, M., B. Johansson, P. Amnéus, and F. Mauss (1998): "Supercharged homogeneous charge compression ignition." In *Proceedings of SEA, International Congress and Exposition*, pp. 1–16. Detroit, MI.

Culick, F. E. C. (1976a): "Nonlinear behavior of acoustic waves in combustion chambers-I." *Acta Astronautica*, **3**, pp. 715–734.

Culick, F. E. C. (1976b): "Nonlinear behavior of acoustic waves in combustion chambers-II." *Acta Astronautica*, **3**, pp. 735–757.

Dowling, A. P. (1999): "A kinematic model of a ducted flame." *Journal of Fluid Mechanics*, **394**, pp. 51–72.

Dowling, A. P. and A. S. Morgans (2005): "Feedback control of combustion oscillations." *Annual Revenue of Fluid Mechanics*, **37**, pp. 151–182.

Dunstan, W. J., R. R. Bitmead, and S. M. Savaresi (2001): "Fitting nonlinear low-order models for combustion instabilitycontrol." *Control Engineering Practice*, **9:12**, pp. 1301–1317.

Egeland, O. and J. T. Gravdahl (2002): *Modeling and Simulation for Automatic Control*. Marine Cybernetics.

Fleifil, M., A. M. Annaswamy, Z. A. Ghoneim, and A. F. Ghoniem (1996): "Responce of a laminar premixed flame to flow oscillations: A kinematic model and thermoacoustic instability result." *Combustion and Flame*, **106**, pp. 487–510.

Fleifil, M., A. M. Annaswamy, J. P. Hathout, and A. F. Ghoniem (1998): "The origin of secondary peaks with active control of thermoacoustic instability." *Combustion Science and Technology*, **133**, June, pp. 227–260.

Franklin, G. F., J. D. Powell, and A. Emami-Naeini (1994): *Feedback Control of Dynamic Systems*. Addison-Wesley, Boston, MA.

Gravdahl, T. (1998): *Modeling and Control of Surge and Rotating Stall Compressors*. PhD thesis Report 98-6-W, Department of Engeneering Cybernetics, Norwegian University of Science and Technology, Trondheim, Norway.

Greitzer, E. M. (1976): "Surge and rotating stall in axial flow compressors, part i: Theoretical compression system model." *Journal of Engineering for Power*, **98**, April, pp. 190–198.

Greitzer, E. M. and F. K. Moore (1986): "A theory of post-stall transients in axial compression systems: Part i - development of equations." *Journal of Engineering for Gas Turbines and Power*, **108**, January, pp. 68–76.

Haugen, F. (1994): *Regulering av dynamiske systemer*. Tapir forlag, Trondheim, Norway.

Haverkamp, B. and M. Verhaegen (1997): *SMI Toolbox, State Space Model Identification Software for Multivariable Dynamical Systems*. Delft University of Technology, Faculty of Information Technology and Systems.

Hermann, J., S. Gleis, and D. Vortmeyer (1996): "Avtive instability control (AIC) of spray combustors by modulation of the liquid fuel flow rate." *Combustion Science and Technology*, **118**, pp. 1–25.

Hermann, J., A. Orthmann, S. Hoffmann, and P. Berenbrink (2000): "Combination of active instability control and passive measures to prevent combustion instabilities in a 260 MW heavy duty gas turbine." In *NATO/PTO/AVT Proceedings of Active Control. Technology Enhanced Performance in Land, Air, and Sea Vehicles*, pp. 1–8. Braunschweig, Germany.

Ikame, M., T. Kishi, K. Harumi, K. Hiraoka, H. Oka, H. Sato, K. Hayashi, C. Nishidome, I. Kajiwara, and S. Ogawa (2005): "Suppression of combustion noise and combustion oscillation by thermoacoustic active control using secondary flame." In *Proceedings of ASME Turbo Expo 2005: Power for Land, Sea and Air*. Reno-Tahoe, NV.

Johansson, R. (1993): *System Modeling and Identification*. Prentice Hall, Englewood Cliffs, NJ.

Khalil, H. K. (2002): *Nonlinear Systems, third edition*. Prentice Hall, Upper Saddle River, NJ.

Langhorne, P. J., A. Dowling, and N. Hooper (1990): "Practical active control system for combustion oscillations." *Journal of Propulsion*, **6:3**, pp. 324–333.

Larimore, W. E. (1983): "System identification, reduced–order filtering and modeling via canonical variate analysys." In *Proceedings of the 1983 American Control Conference*, vol. 2, pp. 445–451. San Francisco, Ca.

Lim, K. W., N. C. Cheung, and M. F. Rahman (1994): "Proportional control of a solenoid actuator." In *Industrial Electronics, Control and Instrumentation, proceedings of the 20th International Conference on*, vol. 3, pp. 2045–2050. Bologna, Italy.

Ljung, L. (2005): *System Identification Toolbox*. The MathWorks, Inc.

MathWorks (2005): *Control System Toolbox*. The MathWorks, Inc.

Merriam-Webster (1987): *Webster's Ninth New Collegiate Dictionary*. Merriam-Webster Inc.

Mijic, D. and C. Stödberg (2004): "Feedback control of thermoacoustic instability using acoustic actuator." Master's thesis ISRN LUTFD2/TFRT--5721--SE. Department of Automatic Control, Lund Institute of Technology, Sweden.

Moore, B. C. (1981): "Principal component analysis in linear systems: Controllability, observability, and model reduction." *IEEE Transactions on Automatic Control*, **AC-26:1**, pp. 17–32.

Morgans, A. S. and A. P. Dowling (2005): "Model–based control of combustion instabilities." In *Proceedings of the ASME Turbo Expo 2005: Power for Land, Sea and Air*, pp. 1–12. Reno-Tahoe, NV.

Neumeier, Y., A. Nabi, A. Arble, M. Vertzberger, and B. T. Zinn (1997): "Open–loop performance of a fast–responce, actively controlled fuel injector actuator." *Journal of Propulsion and Power*, **13:3**, pp. 705–713.

Neumeier, Y. and B. T. Zinn (1996): "Active control of combustion instabilities with real time observation of unstable combustor modes." In *Proceedings of the AIAA 34th Aerospace Sceience Meeting and Exhibit*, pp. 1–19. Reno, NV.

Pernebo, L. and L. M. Silverman (1982): "Model reduction via balanced state space representation." *IEEE Transactions on Automatic Control*, **AC-27:1**, pp. 382–387.

Poinsot, T. and D. Veynante (2001): *Theoretical and Numerical Combustion*. Edwards, Philadelphia, PA, USA.

Prakash, S., S. Nair, T. M. Muruganandam, Y. Neumeier, T. Lieuwen, J. M. Seitzman, and B. T. Zinn (2005): "Acoustic based rapid blowout mitigation in a swirl stabilized combustor." In *Proceedings of ASME Turbo Expo 2005: Power for Land, Sea and Air*. Reno-Tahoe, NV.

Rahman, M. F., N. C. Cheung, and K. W. Lim (1996): "Position estimation in solenoid actuators." *IEEE Transactions on Industry Applications*, **32**, May/June, pp. 552–559.

Rayleigh, M. A. (1877): *The Theory of Sound*. MacMillan & CO, London, UK.

Rayleigh, M. A. (1878): "The explanation of certain acoustical phenomena." *Nature*, July 18, pp. 319–321.

Rijke, P. L. (1859): "Notiz über eine neue Art, die in einer an beiden Enden offenen Röhre enthalten Luft in Schwingungen zu versetzen." *Annalen der Physik und Chemie*, **107**, pp. 339–343.

Riley, A. J., S. Park, A. P. Dowling, S. Evesque, and A. M. Annaswamy (2003): "Adaptive closed-loop control on an atmospheric gaseous lean-premixed combuster." *Proceedings of of the ASME Turbo Expo 2003: Power for Land, Sea and Air*.

Riley, A. J., S. Park, A. P. Dowling, S. Evesque, and A. M. Annaswamy (2004): "Advanced closed-loop control on an atmospheric gaseous lean-premixed combuster." *Journal of Engineering for Gas Turbines and Power*, **126**, October, pp. 708–716.

Rumsey, J. W., M. Fleifil, A. M. Annaswamy, and A. F. Ghoniem (1998): "Low-order nonlinear models of thermoacoustic instabilities and model-based control." In *Proceedings of the 1998 IEEE International Conference on Control Applications*, vol. 2, pp. 1419–1423. Trieste, Italy.

Saravanamuttoo, H. I. H., C. F. C. Rogers, and H. Cohen (2001): *Gas Turbine Theory, Fifth edition*. Pearson, Prentice Hall, Harlow, England.

Shanmugan, K. S. and A. M. Breipohl (1988): *Random Signals, Detection, Estimation and Data Analysis*. John Wiley & Sons, Inc.

Skogestad, S. and I. Postlethwaite (1996): *Multivariable Feedback Control, Analysis and Design*. John Wiley & Sons, UK.

van Overschee, P. and B. de Moor (1996): *Subspace Identification for Linear Systems, Theory - Implementation - Applications*. Kluwer Academic Phulishers, Boston/London/Dordrecht.

Verhaegen, M. (1994): "Identification of the deterministic part of MIMO state space models given in innovations from input-output data." *Automatica*, **30**, pp. 61–74.

Zinn, B. T. (2005): "Smart combusters—just around the corner." In *Proceedings of the ASME Turbo Expo 2005: Power for Land, Sea and Air*, pp. 1–21. Reno-Tahoe, NV.

A

Data Analysis

A.1 Spectrum Analysis

Smoothening of Periodogram

The periodogram is used to illustrate the spectral properties of a data sequence. The analysis of sequences of large sample size results in a high resolution periodogram. To reduce the variance of the estimate, a windowing procedure described in [Shanmugan and Breipohl, 1988] is imposed to smoothen the periodogram. The method ensures asymptotic, unbiased, and consistent estimates when the window length is a fraction of the sample size and the sample size goes to infinity.

Before presenting the algorithm, the discrete Fourier transform and the inverse discrete Fourier transform are presented:

- The discrete Fourier transform (DFT) of the sequence $x_s(k)$ is defined as

$$\mathbf{DFT}(x_s(k), N, l) = \sum_{k=0}^{N-1} x_s(k) e^{-i2\pi kl/N}, \quad l = 0 \cdots N-1 \ .$$

- The inverse discrete Fourier transform (IDFT) of the sequence

$X_d(l)$ is defined as

$$\mathbf{IDFT}(X_d(l), N, k) = \frac{1}{N} \sum_{l=0}^{N-1} X_d(l) e^{i2\pi lk/N}, \quad k = 0 \cdots N-1 \ .$$

If N is a power of two, the DFT and the IDFT can be implemented with the efficient algorithms FFT and IFFT (fast Fourier transform and inverse fast Fourier transform, respectively). Algorithms for FFT and IFFT are implemented in the Matlab® Datafun Toolbox®.

The calculation of the smoothened periodogram is based on the following algorithm

1. Zero–pad the measured data sequence of N so it has the largest power of two above N samples. Denote this sequence $x_s(k)$ and its length N_z.
2. Find the discrete Fourier transform $X_d(l)$ of $x_s(k)$

$$X_d(l) = \mathbf{DFT}(x_s(k), N, l) \quad k = 0 \cdots N_z - 1$$

3. Estimate the autocorrelation function $\widehat{R}_{xx}(d)$ as

$$\widehat{R}_{xx}(d) = \mathbf{IDFT}(\frac{1}{N} X_d {X_d}^*, N, d), \quad d = 0 \cdots (N-1) \ ,$$

where ${X_d}^*$ is the complex conjugated of X_d.

4. Calculate the estimator

$$\begin{aligned} \widehat{R}'_{xx}(d) &= \frac{N-d}{N} \widehat{R}_{xx}(d), \quad d = 0 \cdots N-1 \ , \\ \widehat{R}'_{xx}(-d) &= \widehat{R}'_{xx}(d) \ . \end{aligned}$$

5. Window $\widehat{R}'_{xx}(d)$ by a Bartlett window and truncate for points outside the window

$$\bar{\bar{R}}_{xx}(d) = \widehat{R}'_{xx}(d)\, \Omega(d, M), \quad d = -N+1 \cdots N-1 \ .$$

where M is the window length in the Bartlett window function

$$\Omega(d, M) = \begin{cases} 1 - \frac{|d|}{M} & for \quad d = -M \cdots M \\ 0 & else \end{cases} \ .$$

6. Estimate the smoothened periodogram by

$$\bar{\bar{S}}_{xx}(l) = \mathbf{DFT}(\bar{\bar{R}}_{xx}(d), N, l)\,, \;\; l = 0 \cdots N-1 \;\; .$$

B

Electric Circuit Diagrams

B.1 Circuit Diagram for Valve Driver and Current Measurement

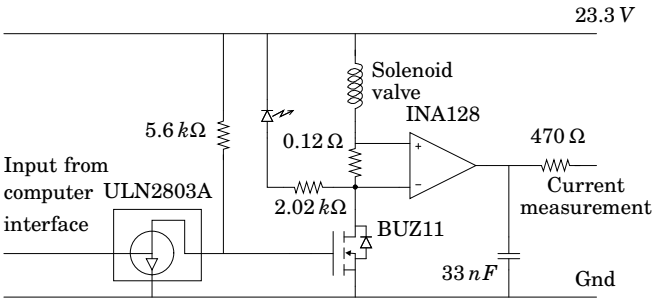

Figure B.1 Circuit diagram for valve driver and current measurement.

B.2 Circuit Diagram for Combustion Chamber Pressure Measurement

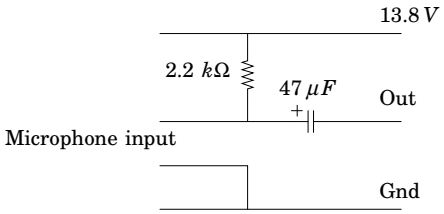

Figure B.2 Circuit diagram for combustion chamber pressure measurement.

B.3 Amplifiers

All signals into the AD–converter are amplified by a amplifier constructed at the Department of Automatic Control by research engineer Rolf Braun. For further details, contact Research engineer Rolf Braun with the reference "*Mätrack, Förstärkare med nollförflyttning*".

Research engineer Rolf Braun

Department of Automatic Control
Lund Institute of Technology
Box 118
S-221 00 Lund, Sweden

URL: http://www.control.lth.se/user/rolfb/welcome-eng.html
Email: Rolf.Braun@control.lth.se
Phone: +46 46 222 9744
Fax: +46 46 13 81 18